

Unveiling the Hidden Structure of Self-Attention via Kernel Principal Component Analysis

Rachel S.Y. Teo Tan M. Nguyen

National University of Singapore
June 21, 2024

Abstract

The remarkable success of transformers in sequence modeling tasks, spanning various applications in natural language processing and computer vision, is attributed to the critical role of self-attention. Similar to the development of most deep learning models, the construction of these attention mechanisms rely on heuristics and experience. In our work, we derive self-attention from kernel principal component analysis (kernel PCA) and show that self-attention projects its query vectors onto the principal component axes of its key matrix in a feature space. We then formulate the exact formula for the value matrix in self-attention, theoretically and empirically demonstrating that this value matrix captures the eigenvectors of the Gram matrix of the key vectors in self-attention. Leveraging our kernel PCA framework, we propose Attention with Robust Principal Components (RPC-Attention), a novel class of robust attention that is resilient to data contamination. We empirically demonstrate the advantages of RPC-Attention over softmax attention on the ImageNet-1K object classification, WikiText-103 language modeling, and ADE20K image segmentation task.

1 Introduction

Transformers [68] have emerged as the preeminent model for tackling a myriad of challenging problems in natural language processing [3, 16, 1, 51, 7, 33, 13], computer vision [18, 64, 37, 48, 32, 20], reinforcement learning [10, 29, 78, 34], and other applications [77, 53, 30, 73]. The effectiveness of transformers is rooted in their ability to learn from unlabeled data and take advantage of pre-trained models for downstream tasks that involve diverse data modalities with limited supervision [49, 50, 74, 81, 52]. At the core of the transformer’s success lies the self-attention mechanism, which serves as the fundamental building block of a transformer model. This mechanism enables each token in a sequence to aggregate information from other tokens by computing a weighted average based on similarity scores between their feature representations. Facilitating dynamic interactions among tokens, this attention mechanism allows tokens to selectively attend to others, thereby attaining a contextual representation [4, 45, 36]. The flexibility in capturing diverse syntactic and semantic relationships is an important factor contributing to the success of transformers [62, 70, 27, 69].

Self-Attention. For a given input sequence $\mathbf{X} := [\mathbf{x}_1, \dots, \mathbf{x}_N]^\top \in \mathbb{R}^{N \times D_x}$ of N feature vectors, self-attention transforms \mathbf{X} into the output sequence \mathbf{H} in the following two steps:

Step 1: The input sequence \mathbf{X} is projected into the query matrix \mathbf{Q} , the key matrix \mathbf{K} , and the value matrix \mathbf{V} via three linear transformations

$$\mathbf{Q} = \mathbf{X}\mathbf{W}_Q^\top; \mathbf{K} = \mathbf{X}\mathbf{W}_K^\top; \mathbf{V} = \mathbf{X}\mathbf{W}_V^\top, \quad (1)$$

where $\mathbf{W}_Q, \mathbf{W}_K \in \mathbb{R}^{D \times D_x}$, and $\mathbf{W}_V \in \mathbb{R}^{D_v \times D_x}$ are the weight matrices. We denote $\mathbf{Q} := [\mathbf{q}_1, \dots, \mathbf{q}_N]^\top$, $\mathbf{K} := [\mathbf{k}_1, \dots, \mathbf{k}_N]^\top$, and $\mathbf{V} := [\mathbf{v}_1, \dots, \mathbf{v}_N]^\top$, where the vectors $\mathbf{q}_i, \mathbf{k}_i, \mathbf{v}_i$ for $i = 1, \dots, N$ are the query, key, and value vectors, respectively.

Step 2: The output sequence $\mathbf{H} := [\mathbf{h}_1, \dots, \mathbf{h}_N]^\top$ is then computed as follows

$$\mathbf{H} = \text{softmax}\left(\mathbf{Q}\mathbf{K}^\top/\sqrt{D}\right)\mathbf{V} := \mathbf{A}\mathbf{V}, \quad (2)$$

where the softmax function is applied to each row of the matrix $\mathbf{Q}\mathbf{K}^\top/\sqrt{D}$. The matrix $\mathbf{A} := \text{softmax}\left(\frac{\mathbf{Q}\mathbf{K}^\top}{\sqrt{D}}\right) \in \mathbb{R}^{N \times N}$ and its component a_{ij} for $i, j = 1, \dots, N$ are called the attention matrix and attention scores, respectively. For each query vector \mathbf{q}_i for $i = 1, \dots, N$, an equivalent form of Eqn. (2) to compute the output vector \mathbf{h}_i is given by

$$\mathbf{h}_i = \sum_{j=1}^N \text{softmax}\left(\mathbf{q}_i^\top \mathbf{k}_j/\sqrt{D}\right) \mathbf{v}_j. \quad (3)$$

The self-attention computed by Eqn. (2) and (3) is called the scaled dot-product or softmax attention. In our paper, we call a transformer that uses this attention the softmax transformer. The structure that the attention matrix \mathbf{A} learns from training determines the ability of the self-attention to capture contextual representations for each token.

Despite their impressive achievements, the development of most attention layers rely on intuitions and heuristic approaches. The quest for a systematic and principled framework for studying and synthesizing attention layers has remained challenging.

Contribution. We study and analyze self-attention in transformers from the perspective of kernel principal component analysis (kernel PCA). In particular, we develop a novel connection between self-attention and kernel PCA, showing that *self-attention projects its query vectors \mathbf{q}_i , $i = 1, \dots, N$, onto principal component axes of the key matrix \mathbf{K} in a feature space.* We then inspect the structure of the value matrix \mathbf{V} of self-attention suggested by our kernel PCA framework, validating *\mathbf{V} captures the eigenvectors of the Gram matrix of the key vectors \mathbf{k}_j , $j = 1, \dots, N$.* Using our framework, we then propose a new class of robust attention, namely the Attention with Robust Principal Components (RPC-Attention). Our contribution is three-fold.

1. We derive self-attention from kernel PCA, showing that the attention outputs are projections of the query vectors onto the principal components axes of the key matrix \mathbf{K} in a feature space.
2. We discover and validate that the value matrix \mathbf{V} in self-attention captures the eigenvectors of the Gram matrix of the key vectors \mathbf{k}_j , $j = 1, \dots, N$.
3. We develop the Attention with Robust Principal Components (RPC-Attention), a new attention mechanism that is resilient to data contamination, using our kernel PCA framework.

We empirically demonstrate the benefits of RPC-Attention on the ImageNet-1K object classification, ADE20K image segmentation, and large scale WikiText-103 language modeling tasks. We further illustrate the robustness of RPC-Attention through our evaluations on popular,

standard robustness benchmarks, as well as various white and black box adversarial attacks on ImageNet-1K images, 15 different types of corruptions on the ADE20K dataset, and word swap attack on WikiText-103.

2 Principal Component Analysis of Attention

In this section, we will derive attention from kernel PCA. Suppose we are given a dataset $M = \{\mathbf{k}_1, \dots, \mathbf{k}_N\} \subset \mathbb{R}^D$. Here, $\mathbf{k}_1, \dots, \mathbf{k}_N$ are attention keys in self-attention. As in kernel PCA, we first project these data points into a feature space using a feature map $\varphi(\mathbf{x}) := \phi(\mathbf{x})/g(\mathbf{x})$, where $\phi(\cdot)$ is a nonlinear transformation from \mathbb{R}^D to $\mathbb{R}^{D'}$, and $g(\cdot)$ is a vector-scalar function that computes a scaling factor for $\phi(\mathbf{x})$. We center the projected data as follows:

$$\tilde{\varphi}(\mathbf{k}_j) = \varphi(\mathbf{k}_j) - \frac{1}{N} \sum_{j'=1}^N \varphi(\mathbf{k}_{j'}). \quad (4)$$

The covariance matrix in the feature space \mathbf{C} is given by

$$\mathbf{C} = \frac{1}{N} \sum_{j=1}^N \tilde{\varphi}(\mathbf{k}_j) \tilde{\varphi}(\mathbf{k}_j)^\top$$

and its eigenvector expansion is

$$\mathbf{C} \mathbf{u}_d = \lambda_d \mathbf{u}_d, \quad d = 1, \dots, D_v. \quad (5)$$

Plugging \mathbf{C} into (5), we obtain

$$\frac{1}{N} \sum_{j=1}^N \tilde{\varphi}(\mathbf{k}_j) \{\tilde{\varphi}(\mathbf{k}_j)^\top \mathbf{u}_d\} = \lambda_d \mathbf{u}_d. \quad (6)$$

Thus, provided that $\lambda_d > 0$, the eigenvector \mathbf{u}_d is given by a linear combination of the $\tilde{\varphi}(\mathbf{k}_j)$ and with $a_{dj} = \frac{1}{N\lambda_d} \tilde{\varphi}(\mathbf{k}_j)^\top \mathbf{u}_d$, can be written as

$$\mathbf{u}_d = \sum_{j=1}^N a_{dj} \tilde{\varphi}(\mathbf{k}_j). \quad (7)$$

2.1 Deriving Attention from Kernel PCA

In order to derive self-attention from kernel PCA, we consider the query vector \mathbf{q}_i in self-attention as a new data point. The projection \mathbf{h}_i of a new test point \mathbf{q}_i onto the principal

components \mathbf{u}_d in Eqn. (7), for $d = 1, \dots, D_v$, is given by

$$\begin{aligned}
\mathbf{h}_i(d) &= \boldsymbol{\varphi}(\mathbf{q}_i)^\top \mathbf{u}_d \\
&= \sum_{j=1}^N a_{dj} \boldsymbol{\varphi}(\mathbf{q}_i)^\top \tilde{\boldsymbol{\varphi}}(\mathbf{k}_j) \\
&= \sum_{j=1}^N a_{dj} \boldsymbol{\varphi}(\mathbf{q}_i)^\top (\boldsymbol{\varphi}(\mathbf{k}_j) - \frac{1}{N} \sum_{j'=1}^N \boldsymbol{\varphi}(\mathbf{k}_{j'})) \\
&= \sum_{j=1}^N \frac{k(\mathbf{q}_i, \mathbf{k}_j)}{g(\mathbf{q}_i)} \frac{a_{dj}}{g(\mathbf{k}_j)} - \frac{1}{N} \sum_{j'=1}^N \frac{k(\mathbf{q}_i, \mathbf{k}_{j'})}{g(\mathbf{q}_i)} \sum_{j=1}^N \frac{a_{dj}}{g(\mathbf{k}_{j'})} \\
&= \sum_{j=1}^N \frac{k(\mathbf{q}_i, \mathbf{k}_j)}{g(\mathbf{q}_i)} \left(\frac{a_{dj}}{g(\mathbf{k}_j)} - \frac{1}{N} \sum_{j'=1}^N \frac{a_{dj'}}{g(\mathbf{k}_{j'})} \right) \\
&= \sum_{j=1}^N \frac{k(\mathbf{q}_i, \mathbf{k}_j)}{g(\mathbf{q}_i)} v_{dj},
\end{aligned} \tag{8}$$

where the kernel $k(\mathbf{x}, \mathbf{y}) := \boldsymbol{\phi}(\mathbf{x})^\top \boldsymbol{\phi}(\mathbf{y})$ and $v_{dj} := \frac{a_{dj}}{g(\mathbf{k}_j)} - \frac{1}{N} \sum_{j'=1}^N \frac{a_{dj'}}{g(\mathbf{k}_{j'})}$. We further let the self-attention's value vectors $\mathbf{v}_j = [v_{1j}, \dots, v_{D_v j}] \in \mathbb{R}^{D_v \times 1}$, $j = 1, \dots, N$, and rewrite the projection \mathbf{h}_i as $\mathbf{h}_i = \sum_{j=1}^N k(\mathbf{q}_i, \mathbf{k}_j)/g(\mathbf{q}_i) \mathbf{v}_j$. Selecting $g(\mathbf{x}) := \sum_{j=1}^N k(\mathbf{x}, \mathbf{k}_j)$ and $k(\mathbf{x}, \mathbf{y}) = \exp(\mathbf{x}^\top \mathbf{y}/\sqrt{D})$, we obtain a formula of an attention:

$$\mathbf{h}_i = \sum_{j=1}^N \frac{k(\mathbf{q}_i, \mathbf{k}_j)}{\sum_{j'=1}^N k(\mathbf{q}_i, \mathbf{k}_{j'})} \mathbf{v}_j = \sum_{j=1}^N \text{softmax}(\mathbf{q}_i^\top \mathbf{k}_j/\sqrt{D}) \mathbf{v}_j. \tag{9}$$

Recovering Self-Attention: Eqn. (9) matches the exact formula of a self-attention as in Eqn. (3). Thus, we can view outputs \mathbf{h}_i of self-attention as projections of the query vectors \mathbf{q}_i , $i = 1, \dots, N$, onto D_v principal components in a feature space:

$$\mathbf{H} = [\boldsymbol{\varphi}(\mathbf{q}_1), \dots, \boldsymbol{\varphi}(\mathbf{q}_N)]^\top [\mathbf{u}_1, \dots, \mathbf{u}_{D_v}]. \tag{10}$$

Computing the Value Vectors: As derived above, the self-attention's value vectors \mathbf{v}_j are given by: $\mathbf{v}_j = [v_{1j}, \dots, v_{D_v j}] \in \mathbb{R}^{D_v \times 1}$, $j = 1, \dots, N$, where $v_{dj} := \frac{a_{dj}}{g(\mathbf{k}_j)} - \frac{1}{N} \sum_{j'=1}^N \frac{a_{dj'}}{g(\mathbf{k}_{j'})}$, $d = 1, \dots, D_v$. Since $g(\mathbf{k}_j)$ can be calculated as $g(\mathbf{k}_j) = \sum_{j'=1}^N k(\mathbf{k}_j, \mathbf{k}_{j'})$, in order to compute \mathbf{v}_j , we need to determine the coefficients $a_{1j}, \dots, a_{D_v j}$ for $j = 1, \dots, N$.

We define $\tilde{k}_\varphi(\mathbf{x}, \mathbf{y}) := \tilde{\boldsymbol{\varphi}}(\mathbf{x})^\top \tilde{\boldsymbol{\varphi}}(\mathbf{y})$ and the Gram matrix $\widetilde{\mathbf{K}}_\varphi \in \mathbb{R}^{N \times N}$ with elements $\widetilde{\mathbf{K}}_\varphi(i, j) = \tilde{k}_\varphi(\mathbf{k}_i, \mathbf{k}_j)$. Substituting the linear expansion in Eqn. (7) into (6), we attain

$$\frac{1}{N} \sum_{j=1}^N \tilde{\boldsymbol{\varphi}}(\mathbf{k}_j) \tilde{\boldsymbol{\varphi}}(\mathbf{k}_j)^\top \sum_{j'=1}^N a_{dj'} \tilde{\boldsymbol{\varphi}}(\mathbf{k}_{j'}) = \lambda_d \sum_{j=1}^N a_{dj} \tilde{\boldsymbol{\varphi}}(\mathbf{k}_j).$$

We multiply both sides of the above by $\tilde{\boldsymbol{\varphi}}(\mathbf{k}_\ell)^\top$ to obtain $\widetilde{\mathbf{K}}_\varphi^2 \mathbf{a}_d = \lambda_d N \widetilde{\mathbf{K}}_\varphi \mathbf{a}_d$, with the column vector $\mathbf{a}_d = [a_{d1}, \dots, a_{dN}]^\top \in \mathbb{R}^{N \times 1}$. We compute \mathbf{a}_d by solving

$$\widetilde{\mathbf{K}}_\varphi \mathbf{a}_d = \lambda_d N \mathbf{a}_d. \tag{11}$$

The calculation of $\widetilde{\mathbf{K}}_\varphi$ is provided in Remark 1. We summarize our results in the following theorem.

Theorem 1 (Softmax Attention as Principal Component Projections) *Given a set M of key vectors, $M := \{\mathbf{k}_1, \dots, \mathbf{k}_N\} \subset \mathbb{R}^D$, a kernel $k(\mathbf{x}, \mathbf{y}) := \exp(\mathbf{x}^\top \mathbf{y} / \sqrt{D})$, and a vector-scalar function $g(\mathbf{x}) := \sum_{j=1}^N k(\mathbf{x}, \mathbf{k}_j)$, self-attention performs kernel PCA and projects a query vector $\mathbf{q}_i \in \mathbb{R}^D$ onto principal component axes of M in an infinite dimensional feature space φ as follows*

$$\mathbf{h}_i = \sum_{j=1}^N \text{softmax}\left(\mathbf{q}_i^\top \mathbf{k}_j / \sqrt{D}\right) \mathbf{v}_j.$$

The feature space φ is induced by the kernel $k_\varphi(\mathbf{x}, \mathbf{y}) := \frac{k(\mathbf{x}, \mathbf{y})}{g(\mathbf{x})g(\mathbf{y})}$, and the value vectors $\mathbf{v}_j = [v_{1j}, \dots, v_{D_v j}] \in \mathbb{R}^{D_v \times 1}$, $j = 1, \dots, N$, where $v_{dj} := \frac{a_{dj}}{g(\mathbf{k}_j)} - \frac{1}{N} \sum_{j'=1}^N \frac{a_{dj'}}{g(\mathbf{k}_j)}$, $d = 1, \dots, D_v$. The column vectors $\mathbf{a}_d = [a_{d1}, \dots, a_{dN}]^\top \in \mathbb{R}^{N \times 1}$ can be determined by solving the eigenvalue problem defined in Eqn. (11). This constraint on \mathbf{v}_j can be relaxed by letting the self-attention learn \mathbf{v}_j from data via a linear projection of the input \mathbf{x}_j , i.e., $\mathbf{v}_j = \mathbf{W}_V \mathbf{x}_j$ where \mathbf{W}_V is a learnable matrix.

Remark 1 (Calculating the Gram Matrix $\widetilde{\mathbf{K}}_\varphi$) In the eigenvalue problem defined in Eqn. (11), the centered Gram matrix $\widetilde{\mathbf{K}}_\varphi$ can be computed from the uncentered Gram matrix \mathbf{K}_φ with elements $\mathbf{K}_\varphi(i, j) = k_\varphi(\mathbf{k}_i, \mathbf{k}_j) = \varphi(\mathbf{k}_i)^\top \varphi(\mathbf{k}_j)$. In particular, $\widetilde{\mathbf{K}}_\varphi = \mathbf{K}_\varphi - \mathbf{1}_N \mathbf{K}_\varphi - \mathbf{K}_\varphi \mathbf{1}_N + \mathbf{1}_N \mathbf{K}_\varphi \mathbf{1}_N$, where $\mathbf{1}_N$ denotes the $N \times N$ matrix in which every element takes the value $1/N$ [6] (See Appendix B). Here, the kernel $k_\varphi(\mathbf{x}, \mathbf{y}) := \frac{k(\mathbf{x}, \mathbf{y})}{g(\mathbf{x})g(\mathbf{y})}$.

Remark 2 (Determining D_v) The feature space φ is infinite dimensional, so we can find infinitely many principal components. However, the number of nonzero eigenvalues of \mathbf{C} in Eqn. (5) cannot exceed N , the number of data points, since \mathbf{C} has rank at most equal to N . Notice that only principal components corresponding to nonzero eigenvalues are used for projections in kernel PCA. Thus, D_v , the number of principal components used for projections as in Eqn. (10), must be less than or equal to N , i.e., $D_v \leq N$.

Remark 3 (Parameterization of the Value Matrix \mathbf{V}) Different parameterizations of the value matrix \mathbf{V} can result in different self-attention architectures. For instance, the projection \mathbf{h}_i of a query vector \mathbf{q}_i onto the principal components \mathbf{u}_d , $d = 1, \dots, D_v$, in Eqn. (8) can be rewritten as

$$\mathbf{h}_i(d) = \sum_{j=1}^N \frac{k(\mathbf{q}_i, \mathbf{k}_j)}{g(\mathbf{q}_i)} \left(\frac{a_{dj}}{g(\mathbf{k}_j)} - \frac{1}{N} \sum_{j'=1}^N \frac{g(\mathbf{k}_{j'})}{g(\mathbf{k}_j)} \frac{a_{dj'}}{g(\mathbf{k}_{j'})} \right).$$

Letting $v_{dj} := \frac{a_{dj}}{g(\mathbf{k}_j)}$ and $s_{jj'} = \frac{g(\mathbf{k}_{j'})}{g(\mathbf{k}_j)}$, we obtain

$$\mathbf{h}_i(d) = \sum_{j=1}^N \frac{k(\mathbf{q}_i, \mathbf{k}_j)}{g(\mathbf{q}_i)} \left(v_{dj} - \frac{1}{N} \sum_{j'=1}^N s_{jj'} v_{dj'} \right).$$

Following the same derivation as above, we can write the projection \mathbf{h}_i as an attention

$$\mathbf{h}_i = \sum_{j=1}^N \text{softmax}\left(\mathbf{q}_i^\top \mathbf{k}_j / \sqrt{D}\right) \left(\mathbf{v}_j - \frac{1}{N} \sum_{j'=1}^N s_{jj'} \mathbf{v}_{j'}\right).$$

The matrix form of this new attention form is as follows:

$$\mathbf{H} = \text{softmax}\left(\mathbf{Q}\mathbf{K}^\top / \sqrt{D}\right) (\mathbf{I} - \mathbf{S})\mathbf{V}, \quad (12)$$

where \mathbf{I} is an identity matrix, and \mathbf{S} is the matrix whose elements $\mathbf{S}(j, j') = \frac{1}{N} s_{jj'}$. We name the self-attention defined by Eqn. (12) the Scaled Attention. Even though the softmax attention in (2) and the Scaled Attention in (12) are mathematically equivalent according to our kernel PCA framework, the training procedure might cause the self-attention models that are derived from different parameterizations to have different performances.

2.2 Analysis on the Convergence of Self-Attention Layers to Kernel PCA

In this section, we discuss empirical justifications that after training, the value vectors \mathbf{v}_j parameterized as a 1-layer linear network, i.e., $\mathbf{v}_j = \mathbf{W}_V \mathbf{x}_j$, $j = 1, \dots, N$, in self-attention converge to the values predicted by our kernel PCA framework in Theorem 1. In other words, we provide evidence that the self-attention layers in transformers try to learn their value vectors \mathbf{v}_j to perform the kernel PCA.

2.2.1 Projection Error Minimization

PCA can be formulated based on projection error minimization as well. In particular, PCA minimizes the average projection cost defined as the mean squared distance between the original data points and their projections [47]. Given our kernel PCA framework in Theorem 1, this implies that self-attention minimizes the following projection error

$$J_{\text{proj}} = \frac{1}{N} \sum_{i=1}^N \|\varphi(\mathbf{q}_i) - \sum_{d=1}^{D_v} h_{di} \mathbf{u}_d\|^2 = \frac{1}{N} \sum_{i=1}^N (\|\varphi(\mathbf{q}_i)\|^2 - \|\mathbf{h}_i\|^2). \quad (13)$$

In the derivation above, we leverage the orthonormality of $\{\mathbf{u}_d\}_{d=1}^{D_v}$ and $h_{di} = \varphi(\mathbf{q}_i)^\top \mathbf{u}_d$. Here, notice that we can compute $\|\varphi(\mathbf{q}_i)\|^2$ from \mathbf{q}_i and $\{\mathbf{k}_j\}_{j=1}^N$ as

$$\|\varphi(\mathbf{q}_i)\|^2 = \exp(\mathbf{q}_i^\top \mathbf{q}_i / \sqrt{D}) / \left(\sum_{j=1}^N \exp(\mathbf{q}_i^\top \mathbf{k}_j / \sqrt{D})\right)^2.$$

In Fig. 1, we empirically show that a transformer model minimizes the projection loss J_{proj} during training. Here, we train a vision transformer [18], ViT-tiny model in particular, on the ImageNet-1K object classification task and compute the average of J_{proj} across attention heads and layers. This result suggests that during training, the transformer learns to perform kernel PCA at each self-attention layer by implicitly minimizing the projection loss J_{proj} .

Thus, the value vector \mathbf{v}_j , $j = 1, \dots, N$, in self-attention layers converge to the values specified in Theorem 1. We provide more details on the computation of J_{proj} in Appendix C.

2.2.2 Learning the Eigenvectors of the Gram Matrix

In this section, we study empirical results that confirm Eqn. (11). In particular, we aim to verify that after training, the value matrix $\mathbf{V} := [\mathbf{v}_1, \dots, \mathbf{v}_N]^\top$ captures the eigenvectors \mathbf{a}_d , $d = 1, \dots, D_v$, of the Gram matrix $\widetilde{\mathbf{K}}_\varphi$.

We first compute \mathbf{a}_d in terms of \mathbf{V} . Recall from Eqn. (11) that $\mathbf{a}_d = [a_{d1}, a_{d2}, \dots, a_{dN}]^\top$. We denote the diagonal matrix $\mathbf{G} := \text{diag}(1/g(\mathbf{k}_1), \dots, 1/g(\mathbf{k}_N))$, the matrix $\mathbf{A} := [\mathbf{a}_1, \dots, \mathbf{a}_{D_v}]$, and rewrite the value vectors \mathbf{v}_j , $j = 1, \dots, N$, as follows:

$$\mathbf{v}_j = \left[\frac{\mathbf{a}_1[j]}{g(\mathbf{k}_j)} - \frac{1}{N} \sum_{j'=1}^N \frac{\mathbf{a}_1[j']}{g(\mathbf{k}_j)}, \dots, \frac{\mathbf{a}_{D_v}[j]}{g(\mathbf{k}_j)} - \frac{1}{N} \sum_{j'=1}^N \frac{\mathbf{a}_{D_v}[j']}{g(\mathbf{k}_j)} \right].$$

The value matrix \mathbf{V} in self-attention is then given by

$$\mathbf{V} = \mathbf{G}\mathbf{A} - \mathbf{G}\mathbf{1}_N\mathbf{A} \Leftrightarrow \mathbf{A} = (\mathbf{I} - \mathbf{1}_N)^{-1}\mathbf{G}^{-1}\mathbf{V}$$

Thus, given the value matrix $\mathbf{V} = \mathbf{X}\mathbf{W}_V^\top$ that the self-attention learns after training, the estimation $\hat{\mathbf{a}}_d$ of \mathbf{a}_d can be computed as

$$\hat{\mathbf{a}}_d = (\mathbf{I} - \mathbf{1}_N)^{-1}\mathbf{G}^{-1}\mathbf{V}[:, d].$$

We empirically verify that $\frac{\widetilde{\mathbf{K}}_\varphi \hat{\mathbf{a}}_d}{N\hat{\mathbf{a}}_d} = \boldsymbol{\gamma} = [\gamma_1, \dots, \gamma_N]$ where $\gamma_1 = \dots = \gamma_N = \text{const}$, which confirms that $\hat{\mathbf{a}}_d$ is an eigenvector of $\widetilde{\mathbf{K}}_\varphi$. In particular, in Fig. 2(Left), we plot the average pairwise absolute differences of γ_i and γ_j , $i \neq j$, $i, j = 1, \dots, N$, for each principal component axis of $\widetilde{\mathbf{K}}_\varphi$. The results are averaged over all attention heads and all layers in the 12-layer ViT-tiny model trained on ImageNet-1K. As can be seen in our figure, the absolute difference between any pair of γ_i and γ_j is almost 0 with a very small standard deviation. Similar results are observed at each layer when averaging over all attention heads in that layer. In Fig. 2(Right), we show the results for Layers 2, 5, 8, and 11 in the model and a plot of all layers is visualized in Appendix E.2. For comparison, we observe that the max, min, mean, and median of the absolute values of these D_v eigenvalues, averaged over all attention heads and layers, are 648.46, 4.65, 40.07, and 17.73, respectively, which are much greater than the values of $|\gamma_i - \gamma_j|$. These results empirically justify that $\frac{\widetilde{\mathbf{K}}_\varphi \hat{\mathbf{a}}_d}{N\hat{\mathbf{a}}_d} = \text{const}$ and the value matrix \mathbf{V} captures the eigenvectors of $\widetilde{\mathbf{K}}_\varphi$ after the transformer model is trained, as suggested in Eqn. (11).

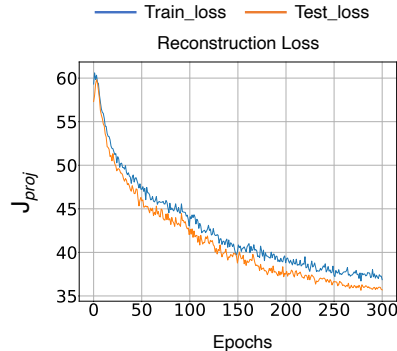


Figure 1: Projection loss vs. training epochs of ViT-tiny model. The reconstruction loss is averaged over the batch, heads, and layers. The downward trend suggests that the model is implicitly minimizing this projection loss.

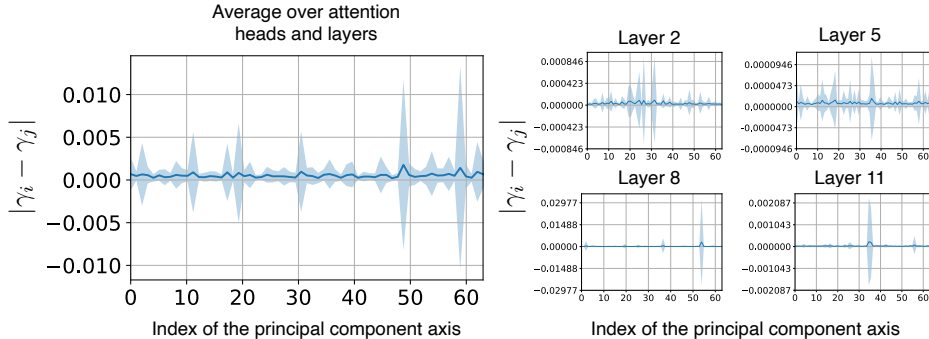


Figure 2: Mean and standard deviation of the absolute differences of elements in the constant vector $\mathbf{1}\lambda_d$, $d = 1, \dots, D_v$. The mean should be 0 with small standard deviations when v_{dj} are close to the values predicted in Theorem 1. For comparison, we observe that the max, min, mean, and median of the absolute values of all the eigenvalues, averaged over all attention heads and layers, are 648.46, 4.65, 40.07, and 17.73, respectively, which are much greater than the values of $|\gamma_i - \gamma_j|$.

In order to prove that after training a transformer with the value vectors \mathbf{v}_j parameterized as $\mathbf{W}_V \mathbf{x}_j$, $j = 1, \dots, N$, using stochastic gradient descent, v_{dj} converges to $\frac{a_{dj}}{g(\mathbf{k}_j)} - \frac{1}{N} \sum_{j'=1}^N \frac{a_{dj'}}{g(\mathbf{k}_{j'})}$ as stated in Theorem 1, it is sufficient to prove that after the training, the outputs \mathbf{h}_i of self-attention become projections of the query vectors \mathbf{q}_i , $i = 1, \dots, N$, onto D_v principal component axes in the feature space φ , i.e., the eigenvectors $\mathbf{u}_1, \dots, \mathbf{u}_{D_v}$ of the covariance matrix \mathbf{C} . To theoretically prove this result for a multi-layer multi-head softmax transformer trained to explicitly minimize a particular loss, e.g., cross-entropy or L2 loss, using stochastic gradient descent is indeed challenging due to the highly nonconvex nature of the optimization problem and the nonlinear structure of the model. Our experimental results in Section 2.2.1 and 2.2.2 empirically justify this result and serve as guidance for the theoretical proof, which we leave for future work.

3 Robust Softmax Attention

In this section, we employ our kernel PCA framework in Section 2 to derive a new class of robust attention, namely, *Attention with Robust Principal Components* (RPC-Attention). It is a well-known problem that both PCA and kernel PCA are sensitive to grossly corrupted data routinely encountered in modern applications [8, 43, 28, 15]. Since self-attention performs kernel PCA by projecting the query vectors \mathbf{q}_i , $i = 1, \dots, N$, onto principal components in a feature space as derived in Section 2.1, it is also vulnerable to data corruption and perturbation. Our RPC-Attention robustifies self-attention by solving a convex program known as Principal Component Pursuit (PCP) [8].

3.1 Principal Component Pursuit

Given corrupted measurement matrix $\mathbf{M} \in \mathbb{R}^{N \times D}$, both PCA and PCP aim to recover a low-rank matrix $\mathbf{L} \in \mathbb{R}^{N \times D}$ from \mathbf{M} . However, while PCA models the corruption by a small Gaussian noise term, PCP models the corruption by a matrix $\mathbf{S} \in \mathbb{R}^{N \times D}$ that can have arbitrarily large magnitude with sparse supports. In particular, PCP solves the following

convex optimization problem:

$$\text{minimize}_{\mathbf{L}, \mathbf{S}} \quad \|\mathbf{L}\|_* + \lambda \|\mathbf{S}\|_1 \quad \text{subject to} \quad \mathbf{L} + \mathbf{S} = \mathbf{M},$$

where $\|\mathbf{L}\|_*$ is the nuclear norm of \mathbf{L} , i.e., the sum of the singular values of \mathbf{L} , and $\|\mathbf{S}\|_1 = \sum_{id} |S_{id}|$ is the ℓ_1 -norm of \mathbf{S} . From [8], under minimal assumptions on the rank and sparsity of \mathbf{L} and \mathbf{S} , the PCP solution exactly recovers the low-rank component \mathbf{L} and the sparse component \mathbf{S} . *Since PCP can recover the principal components of a data matrix even when a positive fraction of the measurements are arbitrarily corrupted, it is more robust than PCA.*

3.2 Attention with Robust Principal Components

In self-attention, following our kernel PCA framework in Section 2, the dataset M is given as $M = \{\mathbf{k}_1, \dots, \mathbf{k}_N\} \subset \mathbb{R}^D$ and $\mathbf{k}_1, \dots, \mathbf{k}_N$ are key vectors. Thus, the key matrix $\mathbf{K} := [\mathbf{k}_1, \dots, \mathbf{k}_N]^\top \in \mathbb{R}^{N \times D}$ in self-attention can be set as the measurement matrix \mathbf{M} in PCP. Then, the PCP for self-attention can be formulated as

$$\text{minimize}_{\mathbf{L}, \mathbf{S}} \quad \|\mathbf{L}\|_* + \lambda \|\mathbf{S}\|_1 \quad \text{subject to} \quad \mathbf{L} + \mathbf{S} = \mathbf{K}. \quad (14)$$

Following [8], we utilize the Alternating Direction Method of Multipliers (ADMM) algorithm introduced in [35, 75] to solve the convex program (14). The augmented Lagrangian of (14) is

$$\mathcal{L}(\mathbf{L}, \mathbf{S}, \mathbf{Y}) = \|\mathbf{L}\|_* + \lambda \|\mathbf{S}\|_1 + \langle \mathbf{Y}, \mathbf{K} - \mathbf{L} - \mathbf{S} \rangle + \mu/2 \|\mathbf{K} - \mathbf{L} - \mathbf{S}\|_F^2.$$

An ADMM solves the convex program (14) by iterating the following steps until convergence: [1] setting $\mathbf{S}_{k+1} = \arg \min_{\mathbf{S}} \mathcal{L}(\mathbf{L}_k, \mathbf{S}, \mathbf{Y}_k)$, [2] setting $\mathbf{L}_{k+1} = \arg \min_{\mathbf{L}} \mathcal{L}(\mathbf{L}, \mathbf{S}_{k+1}, \mathbf{Y}_k)$, and [3] updating the Lagrange multiplier matrix $\mathbf{Y}_{k+1} = \mathbf{Y}_k + \mu(\mathbf{K} - \mathbf{L}_{k+1} - \mathbf{S}_{k+1})$. We define $\mathcal{S}_\tau(x) := \text{sgn}(x) \max(|x| - \tau, 0)$ as an element-wise shrinkage operator and $\mathcal{D}_\tau(\mathbf{X}) = \mathbf{U} \mathcal{S}_\tau(\Sigma) \mathbf{V}^*$ as a singular value thresholding operator with the singular value decomposition of $\mathbf{X} = \mathbf{U} \Sigma \mathbf{V}^*$. As proven in [8], we can rewrite steps [1] and [2] as

$$\begin{aligned} \arg \min_{\mathbf{S}} \mathcal{L}(\mathbf{L}, \mathbf{S}, \mathbf{Y}) &= \mathcal{S}_{\lambda/\mu}(\mathbf{K} - \mathbf{L} + \mu^{-1} \mathbf{Y}) \\ \arg \min_{\mathbf{L}} \mathcal{L}(\mathbf{L}, \mathbf{S}, \mathbf{Y}) &= \mathcal{D}_\mu(\mathbf{K} - \mathbf{S} - \mu^{-1} \mathbf{Y}). \end{aligned}$$

\mathcal{D}_μ finds a low-rank approximation of $\mathbf{K} - \mathbf{S} - \mu^{-1} \mathbf{Y}$. Thus, we obtain an approximation of the above equation by replacing \mathcal{D}_μ by a low-rank approximation operator. Such an approximation takes a step towards the minimum of $\mathcal{L}(\mathbf{L}, \mathbf{S}, \mathbf{Y})$ when fixing \mathbf{S} and \mathbf{Y} . It has been empirically observed and theoretically proven that the output matrix \mathbf{H} of self-attention is low-rank, a phenomenon known as over-smoothing or rank collapse [56, 71, 17]. Therefore, we can replace \mathcal{D}_μ by a self-attention operator. The ADMM method applied to self-attention, which we name *Principal Attention Pursuit* (PAP), is given by Algorithm 1. We define our RPC-Attention as

Algorithm 1 Principal Attention Pursuit (PAP)

initialize: $\mathbf{S}_0 = \mathbf{Y}_0 = \mathbf{0}$; $\mu, \lambda > 0$.
while not converged **do**
 compute $\mathbf{S}_{k+1} = \mathcal{S}_{\lambda/\mu}(\mathbf{K} - \mathbf{L}_k + \mu^{-1} \mathbf{Y}_k)$;
 compute $\mathbf{L}_{k+1} = \text{Softmax}(\mathbf{K} - \mathbf{S}_{k+1} - \mu^{-1} \mathbf{Y}_k, \mathbf{K} - \mathbf{S}_{k+1} - \mu^{-1} \mathbf{Y}_k)$;
 compute $\mathbf{Y}_{k+1} = \mathbf{Y}_k + \mu(\mathbf{K} - \mathbf{L}_{k+1} - \mathbf{S}_{k+1})$;
end while
output: \mathbf{L} .

Definition 1 (Attention with Robust Principal Components) *An RPC-Attention performs the PAP in Algorithm 1 for n iterations with λ as a hyperparameter. For the key matrix $\mathbf{K} \in \mathbb{R}^{N \times D}$, RPC-Attention sets $\mu = ND/4\|\mathbf{K}\|_1$ as suggested in [8], where $\|\mathbf{K}\|_1 = \sum_{id} |K_{id}|$. The output matrix \mathbf{H} of RPC-Attention is set to be the low-rank output matrix \mathbf{L} from PAP.*

4 Experimental Results

We aim to numerically show that: (i) RPC-Attention achieves competitive or even better accuracy than the baseline softmax attention on clean data, and (ii) the advantages of RPC-Attention are more prominent when there is a contamination of samples across different types of data and a variety of tasks. We also validate the performance of the Scaled Attention proposed in Remark 3.

Throughout our experiments, we compare the performance of our proposed models with the baseline softmax attention of the same configuration. All of our results are averaged over 5 runs with different seeds and run on 4 A100 GPU. Details on the models and training settings are provided in Appendix A and additional experimental results are provided in Appendix E. Primarily, we focus on a ViT-tiny model backbone [18], but included in the appendix are experiments on a larger model backbone, ViT-small, and a state of the art (SOTA) robust model, Fully Attentional Networks (FAN) [80].

4.1 Vision Tasks: ImageNet-1K Object Classification

We implement PAP in Algorithm 1 in the symmetric softmax attention layers of a ViT-tiny model and compare it to the standard symmetric model as our baseline. We refer to our model as RPC-SymViT and the baseline model as SymViT. For RPC-SymViT, we study two settings. In the first setting, which we denote by RPC-SymViT (*niter/layer1*), $n = 4, 5, 6$, to maintain the computational efficiency of the model, we apply n PAP iterations only at the first layer to recover a cleaner data matrix that is then sent to the subsequent layers in the model. In the second setting, which we denote by RPC-SymViT (*niter/all-layer*), $n = 2$, we apply n PAP iterations at all layers. We note that an iterative scheme has the potential to have an increased computational load, hence, we provide a comparison on the number of flops per sample, run time per sample, memory and number of parameters between RPC-SymViT and the baseline in Appendix E.8, showing a comparable efficiency.

Robustness against Data Corruptions. To benchmark robustness to data corruptions, we use the standard datasets, ImageNet-C (IN-C) [25], ImageNet-A (IN-A), ImageNet-O (IN-O) [26], and ImageNet-R (IN-R) [24]. We provide details on each dataset and the metrics for evaluation in Appendix A.1. The direction of increasing or decreasing values of these metrics signifying greater robustness are indicated in the Table 1 with an arrow, along with the results on each dataset.

Across all evaluations, RPC-SymViT outperforms the SymViT baseline, thereby justifying the advantages of our RPC-Attention. Particularly, RPC-SymViT with 6 iterations in the 1st layer achieves an improvement of over 1% in terms of accuracy on the clean ImageNet-1K validation set and almost 3 AUPR on ImageNet-O compared to the SymViT. This result is consistent with the intuition that a higher number of iterations executed on a consistent

Table 1: Top-1, Top-5 accuracy (%) , mean corruption error (mCE), and area under the precision-recall curve (AUPR) of RPC-SymViT and SymViT on clean ImageNet-1K data and popular standard robustness benchmarks for image classification. RPC-SymViT (*niter/layer1*) applies n PAP iterations only at the first layer. RPC-SymViT (*niter/all-layer*) applies n PAP iterations at all layers.

Model	IN-1K		IN-R	IN-A	IN-C		IN-O
	Top-1 \uparrow	Top-5 \uparrow	Top-1 \uparrow	Top-1 \uparrow	Top-1 \uparrow	mCE \downarrow	AUPR \uparrow
SymViT (baseline)	70.44	90.17	28.98	6.51	41.45	74.75	17.43
RPC-SymViT (4iter/layer1)	70.94	90.47	29.99	6.96	42.35	73.58	19.32
RPC-SymViT (5iter/layer1)	71.31	90.59	30.28	7.27	42.43	73.43	20.35
RPC-SymViT (6iter/layer1)	71.49	90.68	30.03	7.33	42.76	73.03	20.29
RPC-SymViT (2iter/all-layer)	70.59	90.15	29.23	7.55	41.64	74.52	19.18

Table 2: Top-1/5 accuracy (%) on attacked ImageNet-1K data. RPC-SymViT (*niter/layer1*) applies n PAP iterations at the first layer. RPC-SymViT (*niter/all-layer*) applies n PAP iterations at all layers.

Attack	Metric/Model	SymViT	RPC-SymViT	RPC-SymViT	RPC-SymViT	RPC-SymViT
		(baseline)	(4iter/layer1)	(5iter/layer1)	(6iter/layer1)	(2iter/all-layer)
PGD	Top-1 \uparrow	4.98	5.15	5.11	5.20	6.12
	Top-5 \uparrow	10.41	11.20	11.13	11.34	13.24
FGSM	Top-1 \uparrow	23.38	26.62	26.75	27.22	29.20
	Top-5 \uparrow	53.82	56.87	57.19	57.55	59.63
SPSA	Top-1 \uparrow	47.94	48.13	49.29	48.75	51.01
	Top-5 \uparrow	82.63	82.87	83.52	83.27	83.66
SLD	Top-1 \uparrow	67.91	68.48	68.60	68.99	67.60
	Top-5 \uparrow	89.68	90.16	90.18	90.38	89.79
CW	Top-1 \uparrow	48.44	50.00	50.08	50.36	48.77
	Top-5 \uparrow	72.68	74.24	74.14	74.46	72.91
Noise	Top-1 \uparrow	67.81	68.37	68.72	68.81	68.09
	Top-5 \uparrow	88.51	89.00	89.13	89.27	88.64
AutoAttack	Top-1 \uparrow	23.09	24.56	24.68	24.74	23.51
	Top-5 \uparrow	63.48	65.11	65.09	65.13	64.06

data matrix leads to cleaner data. The full details of all corruption types are presented in Appendix E.3.

Robustness under Adversarial Attacks. We report the top-1 and top-5 accuracy of the models on ImageNet-1K distorted by white box attacks, including PGD [39], FGSM [23], SLD [65], and CW [9] attacks. We further examine the models on the black-box attack SPSA [67], AutoAttack [14], and a noise-adding attack. In Table 2, we present the results of all attacks, where PGD and FGSM are reported for the maximum perturbation budget.

On all attacks, RPC-SymViT outperforms SymViT by a substantial margin, demonstrating the effectiveness of RPC-Attention. Notably, as the square attack in AutoAttack is also a score-based black box attack, in order to further verify our method, we include the results

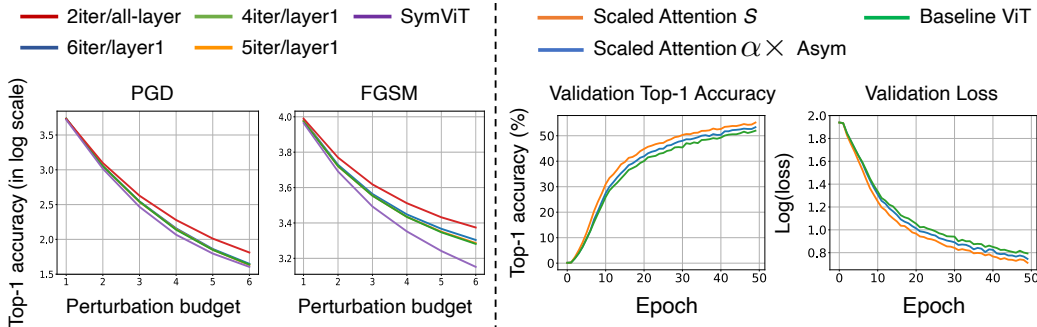


Figure 3: **Left:** Top-1 accuracy of RPC-SymViT vs. baseline SymViT evaluated on PGD/FGSM attacked ImageNet-1K validation set across increasing perturbation budgets. **Right:** Validation top-1 accuracy (%) and loss of Scaled Attention vs. the baseline asymmetric softmax attention in ViT for the first 50 training epochs.

of RPC-SymViT (6iter/layer1) and the baseline SymViT on this attack in the Appendix E.4 in which our model also performs better. This result together with our model’s considerable improvement over the baseline on the black-box SPSA attack justifies that RPC-Attention’s robustness against adversarial attacks is not due to any form of gradient masking. In addition, we illustrate RPC-SymViT’s robustness across increasing perturbations for PGD and FGSM in Fig. 3(left). Details on the evaluation of the models under all attacks are provided in Appendix A.2.

ADE20K Image Segmentation. We continue evaluating the benefits of our method by implementing RPC-Attention in a Segmester model [57] and providing results on the ADE20K image segmentation task [79]. Table 6 in Appendix A.3 shows that Segmester with the RPC-SymViT backbone outperforms the Segmester with the baseline SymViT backbone on both clean and corrupted data.

4.2 Language Tasks: WikiText-103 Language Modeling

We assess our model on the large-scale WikiText-103 language modeling task [41]. Using a standard transformer language model [68], with a symmetric attention layer (SymLm), we replace it with an RPC-Attention layer (RPC-SymLm). As with RPC-SymViT, we only implement RPC-Attention in the first four layers of SymLm and run PAP for 4 iterations to save on computational overhead. The results of the validation and test perplexity (PPL) summarized in Table 3 validate the advantage of our method, surpassing the baseline by at least 1 PPL for all datasets.

4.3 Validating the Benefits of Scaled Attention

In this section, we provide an empirical comparison between the Scaled Attention in Remark 3 and the softmax attention. We train an asymmetric ViT-tiny model with two different versions of Scaled Attention. While the exact value of S can be mathematically formulated as in Remark 3, it might lead to numerical errors that are difficult to handle. Therefore, in the first version of Scaled Attention, we let S be a learned parameter matrix in each layer (Scaled Attention S in Fig. 3(right)). In the second version of Scaled Attention (Scaled Attention $\alpha \times$ Asym in Fig. 3(right)), given that $s_{j'j} = g(k_{j'})/g(k_j)$, we rewrite S as the product of a symmetric softmax

attention matrix and the reciprocal of its transpose. The model learns this reciprocal by a learnable scalar α and we let $\mathbf{S} = \alpha \mathbf{A}_{Sym}$, where \mathbf{A}_{Sym} is the symmetric softmax attention. More details are in Appendix E.1.

Fig. 3(right) shows the top-1 validation accuracy and loss over 50 epochs when training ViT models equipped with Scaled Attention and softmax attention on the ImageNet-1K object classification task. The full training curve can also be found in Appendix E.1. The results suggest that both versions of Scaled Attention outperform the softmax attention. This provides further evidence that self-attention learns to approximate a kernel PCA since the Scaled Attention with a more explicit structure of the value matrix \mathbf{V} suggested in Theorem 1 obtains better performance than softmax attention.

5 Related Works

Theoretical Perspectives of Attention Mechanisms. The study of the attention mechanism in transformers through different theoretical frameworks has been expanding. [66] shows that attention can be analyzed as a kernel smoother over the inputs using an appropriate kernel score that is the similarities between them. [12, 72, 31] reduce the quadratic complexity of transformers by linearizing the softmax kernel to improve the computational and memory efficiency. In addition, there are works interpreting transformers using the frameworks of ordinary/partial differential equations [38, 54, 22, 21] and from probabilistic viewpoints with Gaussian Mixture Models [19, 60, 76]. [11] provides a new perspective by emphasizing the asymmetry of the softmax kernel and recovers the self-attention mechanism from an asymmetric Kernel Singular Value Decomposition (KSVD) using the duality of the optimization problem. Another related work views transformers from the perspective of Support Vector Machines [61]. We discuss [11] and [61] in more details in Appendix F. Separate from these works, our kernel PCA perspective derives softmax attention as a projection of the query vectors in a feature space. Using our framework, we are able to predict the exact explicit form of the value matrix in self-attention, demonstrating that this matrix captures the eigenvectors of the Gram matrix of the key vectors in a feature space. Our work is the first to show this insight.

Robustness of Transformers. There have been many works studying the robustness of Vision Transformers (ViT) [18] against different types of attacks [5, 46, 58, 80]. Recent work that serves to address this include [40], whereby new training strategies and architectural adjustments are proposed to improve the robustness of ViT. Our RPC-Attention is orthogonal to these methods.

6 Concluding Remarks

In this paper, we derive self-attention from kernel principal component analysis (kernel PCA) as a projection of the query vectors onto the principal component axes of the key matrix in a

Table 3: Validation/test perplexity (PPL) on clean WikiText-103 and word swap attacked dataset. RPC-Symlm ($niter/layern_1-n_2$) applies n iterations of PAP only in layers n_1 to n_2 of the model.

Model	Wikitext-103		Attacked Wikitext-103	
	Valid-ppl ↓	Test-ppl ↓	Valid-ppl ↓	Test-ppl ↓
Symlm	38.37	36.36	42.90	44.32
RPC-Symlm (4iter/layer1-4)	37.38	35.26	41.83	43.16

feature space. Using our kernel PCA framework, we derive a new class of robust attention, namely the Attention with Robust Principal Components (RPC-Attention), that is resilient to data contamination. A limitation of RPC-Attention is its derivation from an iterative algorithm that leads to its unrolling architecture, increasing the computational cost of the model. In our paper, we mitigate this by only replacing softmax attention with RPC-Attention in the first layer of the model and demonstrate that doing so is sufficiently effective for robustness. In addition, we provide a comparison of the efficiency of RPC-Attention with softmax attention in Appendix E.8 and find that we are comparable across all metrics at test time while only slightly less efficient during training. It is also interesting to extend our kernel PCA framework to explain multi-layer transformers. We leave these exciting directions as future work.

Supplement to “Unveiling the Hidden Structure of Self-Attention via Kernel Principal Component Analysis”

A Experiment Details

Implementation Details of RPC-SymViT: Our RPC-SymViT models have 5.2M parameters, the same as the SymViT baseline. We use a standard tiny configuration with 12 transformer layers, 3 attention heads per layer, and a model dimension of 192 and simply replace softmax attention with RPC-Attention. We follow the training settings as in [63] and their implementation is available at <https://github.com/facebookresearch/deit>. In a Segmenter model, we use the same RPC-SymViT setting to replace the baseline SymViT backbone. We follow the training details in [57] and their code is publicly available as well, <https://github.com/rstrudel/segmenter>.

There are 3 hyperparameters: 1) μ : this parameter controls the singular value thresholding operator in the PAP algorithm. We set μ to the recommended value given in Definition 1; 2) λ : this is a regularization parameter that controls the sparsity of the corruption matrix \mathbf{S} . We finetune λ for training and observe that RPC-SymViT with $\lambda = 3$ yields the best performance for models with 2 iterations per layer and $\lambda = 4$ yields the best performance for models with iterations only in the first layer; 3) n : the number of iterations of the PAP algorithm in a RPC-Attention layer.

Implementation Details of RPC-Symlm: For our language model, we use a standard transformer language model [68], with a symmetric attention layer. The model has a dimension of 128 for the keys, queries and values, while the training and evaluation context length is set at 256. There are 16 layers altogether and 8 heads per layer. Similarly, we replace the softmax attention with RPC-Attention only in the first four layers to save on computational overhead. There are the same 3 hyperparameters as in RPC-SymViT and we use the same value for μ , $\lambda = 4$ and $n = 4$. We also follow the standard training settings as in [55, 41] and the code base developed by [55], available here <https://github.com/IDSIA/lmtool-fwp>.

A.1 Robustness against Data Corruptions

Datasets: We use the ImageNet-1K dataset that contains 1.28M training images and 50K validation images. There are 1000 classes of images and the model learns an image classification task. For robustness to common corruptions, we use ImageNet-C (IN-C) [25] which consists of 15 different types of corruptions applied to the ImageNet-1K validation set with 5 levels of severity. To test robustness to both input data distribution shifts as well as label distribution shifts, we use ImageNet-A (IN-A) and ImageNet-O (IN-O) [26] respectively. Both of these datasets contain a 200 class subset of ImageNet-1K classes with adversarially filtered images. Finally, we test our model on ImageNet-R (IN-R) [24] which contains various artistic renditions of images. This evaluates the model’s generalization ability to abstract visual renditions.

Metrics: On ImageNet-1K, ImageNet-C, ImageNet-A and ImageNet-R, we report the top-1 accuracies for all experiments. We include top-5 accuracies on ImageNet-1K. On ImageNet-C, the standard metric for evaluation is the mean Corruption Error (mCE). To calculate this,

we average the top-1 error rate for each corruption type across the 5 levels of severity and divide them by AlexNet’s average errors, then take the final average across all corruption types. We report the area under the precision-recall curve (AUPR) for ImageNet-O which requires anomaly scores. The score is obtained by taking the negative of the highest softmax probability output by the model. The direction of increasing or decreasing values of these metrics signifying greater robustness will be indicated in the table with an arrow.

A.2 Robustness under Adversarial Attacks

Attacks: We evaluate the robustness of our method against adversarial attacks using CleverHans [44] and AutoAttack [14]. All attacks are executed on ImageNet-1K’s validation set, and each model is evaluated on the whole set. In particular, we use untargeted, white box attacks such as PGD, FGSM, SLD and CW. In addition, we provide results on gradient-free black box attack, SPSA, diverse AutoAttack, in the standard setting and a simple noise-adding attack. AutoAttack consists of untargeted APGD-CE, targeted APGD-DLR, targeted Fast Adaptive Boundary (FAB) and Square Attack. For further justification of the benefit of our method, we evaluate a variant of our model, RPC-SymViT (6iter/layer1) solely on the black-box Square attack and show that we are robust against black box attacks as well. This is provided in Appendix E.4. We use a perturbation budget of $\epsilon = 1/255$ with the l_∞ norm to manipulate the images and evaluate each model with an incremental increase of $1/255$ in perturbation for PGD and FGSM. In SPSA, we run 40 steps per attack with a perturbation budget of $\epsilon = 0.1$. PGD attack uses a step size of $\alpha = 0.15$ for 20 steps, where at each step the image is adjusted slightly to maximize the model’s loss. Similarly, FGSM does this for a single step. For each attack, we report the top-1 and top-5 accuracy of the model on the distorted dataset with the maximum perturbation budget in Table 2 and across all different perturbations in Figure 3.

A.3 ADE20K Image Segmentation

Dataset: The ADE20K dataset includes complex scenes featuring highly detailed labels, making it one of the most challenging segmentation tasks. The training set contains 20,210 images spread across 150 distinct semantic categories. The validation set includes 2,000 images, while the test set comprises 3,352 images. The metrics report for this task are the Mean Accuracy (%) and Mean Intersection-Over-Union (IOU).

A.4 WikiText-103 Language Modeling

Dataset: The WikiText-103 dataset [41] is derived from Wikipedia articles and is designed to capture long-range contextual dependencies. The training set contains about 28,000 articles, with a total of 103 million words. Each article is divided into text blocks with approximately 3,600 words. The validation and test sets have 218,000 and 246,000 words, respectively, with both sets comprising 60 articles and totaling about 268,000 words. For evaluation, we use a batch size of 1 and apply a sliding window of length L to process the text sequences. When calculating perplexity (PPL), we focus only on the final position, except in the first segment, where we evaluate all positions. We corrupt the both validation and test datasets to demonstrate the robustness of RPC-Attention using TextAttack’s word swap attack [42] to create the attacked WikiText-103 dataset. This adversarial attack randomly replaces words in

the dataset with a generic “AAA” for evaluation making it difficult for the model to predict the next word in the sequence correctly.

B Calculating the Gram Matrix $\widetilde{\mathbf{K}}_\varphi$

In this section, we will show that the centered Gram matrix $\widetilde{\mathbf{K}}_\varphi$ can be computed from the uncentered Gram matrix \mathbf{K}_φ with elements $\mathbf{K}_\varphi(i, j) = k_\varphi(\mathbf{k}_i, \mathbf{k}_j) = \varphi(\mathbf{k}_i)^\top \varphi(\mathbf{k}_j)$. In particular, $\widetilde{\mathbf{K}}_\varphi = \mathbf{K}_\varphi - \mathbf{1}_N \mathbf{K}_\varphi - \mathbf{K}_\varphi \mathbf{1}_N + \mathbf{1}_N \mathbf{K}_\varphi \mathbf{1}_N$, where $\mathbf{1}_N$ denotes the $N \times N$ matrix in which every element takes the value $1/N$. Our centered feature vector has the form

$$\tilde{\varphi}(\mathbf{k}_j) = \varphi(\mathbf{k}_j) - \frac{1}{N} \sum_{j'=1}^N \varphi(\mathbf{k}_{j'}).$$

Then the elements of the centered Gram matrix are given as follows

$$\begin{aligned} \widetilde{\mathbf{K}}_\varphi(i, j) &= \tilde{k}_\varphi(\mathbf{k}_i, \mathbf{k}_j) \\ &= \tilde{\varphi}(\mathbf{k}_i)^\top \tilde{\varphi}(\mathbf{k}_j) \\ &= \varphi(\mathbf{k}_i)^\top \varphi(\mathbf{k}_j) - \frac{1}{N} \sum_{j'=1}^N \varphi(\mathbf{k}_i)^\top \varphi(\mathbf{k}_{j'}) - \frac{1}{N} \sum_{j'=1}^N \varphi(\mathbf{k}_{j'})^\top \varphi(\mathbf{k}_j) + \frac{1}{N^2} \sum_{j'=1}^N \sum_{l=1}^N \varphi(\mathbf{k}_{j'})^\top \varphi(\mathbf{k}_l) \\ &= k_\varphi(\mathbf{k}_i, \mathbf{k}_j) - \frac{1}{N} \sum_{j'=1}^N k_\varphi(\mathbf{k}_i, \mathbf{k}_{j'}) - \frac{1}{N} \sum_{j'=1}^N k_\varphi(\mathbf{k}_{j'}, \mathbf{k}_j) + \frac{1}{N^2} \sum_{j'=1}^N \sum_{l=1}^N k_\varphi(\mathbf{k}_{j'}, \mathbf{k}_l) \end{aligned}$$

which expressed in matrix form, gives the result.

C Plotting J_{proj} in Section 2.2.1

In Section 2.2.1, we plotted the reconstruction loss at each epoch of training. Here, we provide the details of the calculation of this loss. From Eqn. (13),

$$\begin{aligned} L &= \frac{1}{N} \sum_{i=1}^N \left\| \varphi(\mathbf{q}_i) - \sum_{d=1}^{D_v} h_{id} u_d \right\|^2 \\ &= \frac{1}{N} \sum_{i=1}^N (\|\varphi(\mathbf{q}_i)\|^2 - \|\mathbf{h}_i\|^2). \end{aligned}$$

In the above, \mathbf{h}_i is simply our attention output and $\|\varphi(\mathbf{q}_i)\|^2 = \varphi(\mathbf{q}_i)^\top \varphi(\mathbf{q}_i) = \frac{e^{\mathbf{q}_i^\top \mathbf{q}_i / \sqrt{D}}}{(\sum_{j=1}^N e^{\mathbf{q}_i^\top \mathbf{k}_j / \sqrt{D}})^2}$ for $i = 1, \dots, N$, can be calculated using the kernel trick as follows. Let \mathbf{A} be the softmax

attention matrix, \mathbf{a}_1 its first column and \mathbf{a}_1^2 denote the element-wise product.

$$\begin{aligned}
\log(\mathbf{a}_1^2) &= \log\left(\begin{bmatrix} \frac{e^{2\mathbf{q}_1^\top \mathbf{k}_1/\sqrt{D}}}{(\sum_{j=1}^N e^{\mathbf{q}_1^\top \mathbf{k}_j/\sqrt{D}})^2} \\ \vdots \\ \frac{e^{2\mathbf{q}_N^\top \mathbf{k}_1/\sqrt{D}}}{(\sum_{j=1}^N e^{\mathbf{q}_N^\top \mathbf{k}_j/\sqrt{D}})^2} \end{bmatrix}\right) \\
&= \log\left(\begin{bmatrix} e^{2\mathbf{q}_1^\top \mathbf{k}_1/\sqrt{D}} \\ \vdots \\ e^{2\mathbf{q}_N^\top \mathbf{k}_1/\sqrt{D}} \end{bmatrix}\right) - \log\left(\begin{bmatrix} (\sum_{j=1}^N e^{\mathbf{q}_1^\top \mathbf{k}_j/\sqrt{D}})^2 \\ \vdots \\ (\sum_{j=1}^N e^{\mathbf{q}_N^\top \mathbf{k}_j/\sqrt{D}})^2 \end{bmatrix}\right) \\
\Rightarrow \log\left(\begin{bmatrix} (\sum_{j=1}^N e^{\mathbf{q}_1^\top \mathbf{k}_j/\sqrt{D}})^2 \\ \vdots \\ (\sum_{j=1}^N e^{\mathbf{q}_N^\top \mathbf{k}_j/\sqrt{D}})^2 \end{bmatrix}\right) &= \log\left(\begin{bmatrix} e^{2\mathbf{q}_1^\top \mathbf{k}_1/\sqrt{D}} \\ \vdots \\ e^{2\mathbf{q}_N^\top \mathbf{k}_1/\sqrt{D}} \end{bmatrix}\right) - \log(\mathbf{a}_1^2) \\
&= \begin{bmatrix} 2\mathbf{q}_1^\top \mathbf{k}_1/\sqrt{D} \\ \vdots \\ 2\mathbf{q}_N^\top \mathbf{k}_1/\sqrt{D} \end{bmatrix} - \log(\mathbf{a}_1^2) \\
\Rightarrow \begin{bmatrix} (\sum_{j=1}^N e^{\mathbf{q}_1^\top \mathbf{k}_j/\sqrt{D}})^2 \\ \vdots \\ (\sum_{j=1}^N e^{\mathbf{q}_N^\top \mathbf{k}_j/\sqrt{D}})^2 \end{bmatrix} &= e^{\begin{bmatrix} 2\mathbf{q}_1^\top \mathbf{k}_1/\sqrt{D} \\ \vdots \\ 2\mathbf{q}_N^\top \mathbf{k}_1/\sqrt{D} \end{bmatrix} - \log(\mathbf{a}_1^2)}
\end{aligned}$$

Then,

$$\begin{bmatrix} \|\varphi(\mathbf{q}_1)\|^2 \\ \vdots \\ \|\varphi(\mathbf{q}_N)\|^2 \end{bmatrix} = \begin{bmatrix} e^{\mathbf{q}_1^\top \mathbf{q}_1/\sqrt{D}} \\ \vdots \\ e^{\mathbf{q}_N^\top \mathbf{q}_N/\sqrt{D}} \end{bmatrix} / e^{\begin{bmatrix} 2\mathbf{q}_1^\top \mathbf{k}_1/\sqrt{D} \\ \vdots \\ 2\mathbf{q}_N^\top \mathbf{k}_1/\sqrt{D} \end{bmatrix} - \log(\mathbf{a}_1^2)}$$

D Principal Component Pursuit

Let $\mathbf{M}, \mathbf{L}, \mathbf{S} \in \mathbb{R}^{N \times D}$ be the matrix of our corrupted measurements, the low-rank matrix we seek to recover and a sparse corruption matrix respectively. The optimization problem we

would like to solve is

$$\begin{aligned} & \text{minimize}_{\mathbf{L}, \mathbf{S}} && \|\mathbf{L}\|_* + \lambda \|\mathbf{S}\|_1 \\ & \text{subject to} && \mathbf{L} + \mathbf{S} = \mathbf{M} \end{aligned} \tag{15}$$

Under minimal assumptions that the low-rank component \mathbf{L} is not sparse (i.e., \mathbf{L} satisfies the incoherence condition defined in [8]), and the sparse component \mathbf{S} is not low-rank (i.e., the sparsity pattern of \mathbf{S} is selected uniformly at random), we will follow the author’s choice of algorithm to solve the PCP which is to use the Alternating Direction Method of Multipliers (ADMM).

The ADMM algorithm uses the augmented Lagrangian,

$$l(\mathbf{L}, \mathbf{S}, \mathbf{Y}) = \|\mathbf{L}\|_* + \lambda \|\mathbf{S}\|_1 + \langle \mathbf{Y}, \mathbf{M} - \mathbf{L} - \mathbf{S} \rangle + \mu/2 \|\mathbf{M} - \mathbf{L} - \mathbf{S}\|_F^2$$

and solves a sequence of optimization problems. We iterate through $\mathbf{S}_{k+1} = \arg \min_{\mathbf{S}} l(\mathbf{L}_k, \mathbf{S}, \mathbf{Y}_k)$ and $\mathbf{L}_{k+1} = \arg \min_{\mathbf{L}} l(\mathbf{L}, \mathbf{S}_{k+1}, \mathbf{Y}_k)$ before updating the Lagrange multiplier matrix $\mathbf{Y}_{k+1} = \mathbf{Y}_k + \mu(\mathbf{M} - \mathbf{L}_{k+1} - \mathbf{S}_{k+1})$. The advantage of the algorithm is that it turns a complicated optimisation problem into sub problems that have straightforward and efficient solutions. Without much difficulty we can show that:

$$\begin{aligned} \arg \min_{\mathbf{S}} l(\mathbf{L}, \mathbf{S}, \mathbf{Y}) &= \mathcal{S}_{\lambda/\mu}(\mathbf{M} - \mathbf{L} + \mu^{-1}\mathbf{Y}) \\ \arg \min_{\mathbf{L}} l(\mathbf{L}, \mathbf{S}, \mathbf{Y}) &= \mathcal{D}_{\mu}(\mathbf{M} - \mathbf{S} - \mu^{-1}\mathbf{Y}) \end{aligned}$$

where $\mathcal{S}_{\tau}(x) = \text{sgn}(x) \max(|x| - \tau, 0)$ is the shrinkage operator, extended to matrices by applying it element-wise and $\mathcal{D}_{\tau}(\mathbf{X}) = \mathbf{U}\mathcal{S}_{\tau}(\Sigma)\mathbf{V}^*$ is the singular value thresholding operator with the singular value decomposition of $\mathbf{X} = \mathbf{U}\Sigma\mathbf{V}^*$.

The algorithm is summarised as below

Algorithm 2 ADMM for Principal Components Pursuit

initialize: $\mathbf{S}_0 = \mathbf{Y}_0 = \mathbf{0}$; $\mu, \lambda > 0$.
while not converged **do**
 compute $\mathbf{S}_{k+1} = \mathcal{S}_{\lambda/\mu}(\mathbf{M} - \mathbf{L}_k + \mu^{-1}\mathbf{Y}_k)$;
 compute $\mathbf{L}_{k+1} = \mathcal{D}_{\mu}(\mathbf{M} - \mathbf{S}_{k+1} - \mu^{-1}\mathbf{Y}_k)$;
 compute $\mathbf{Y}_{k+1} = \mathbf{Y}_k + \mu(\mathbf{M} - \mathbf{L}_{k+1} - \mathbf{S}_{k+1})$;
end while
output: \mathbf{L}, \mathbf{S} .

E Additional Experimental Results

E.1 Reparameterization of Self-Attention

Let $\mathbf{A}_{sym} = [a_{ij}]$ be the symmetric softmax attention matrix. Then, from Remark 3, \mathbf{S} has the following form and we multiply the numerator and denominator by $1/K(\mathbf{k}_j, \mathbf{k}_{j'})$ to obtain

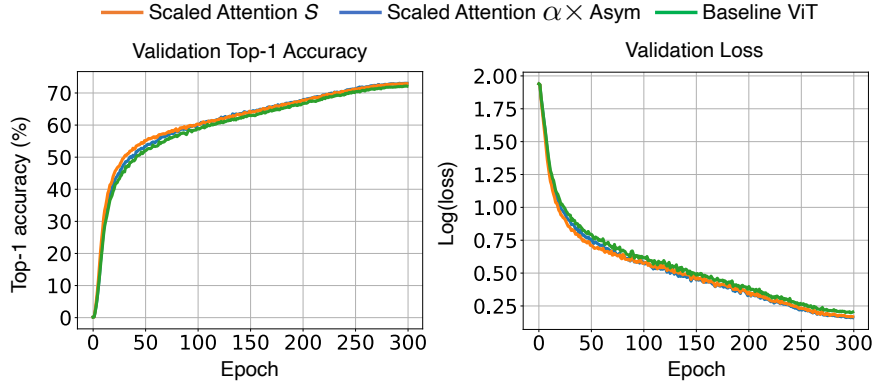


Figure 4: Plot of the validation top-1 accuracy (%) and loss on a log scale of the baseline asymmetric attention ViT and two variants with the parameterization of Remark. 3. The curves are plotted for the full training time and show \mathbf{S} trained as a matrix parameter as well as a scalar parameter scaling a symmetric attention matrix.

a much more convenient expression.

$$\begin{aligned}
 s_{j'j} &= \frac{g(\mathbf{k}_j)}{g(\mathbf{k}_{j'})} \\
 &= \frac{g(\mathbf{k}_j)}{g(\mathbf{k}_{j'})} \times \frac{1/K(\mathbf{k}_j, \mathbf{k}_{j'})}{1/K(\mathbf{k}_j, \mathbf{k}_{j'})} \\
 &= \frac{g(\mathbf{k}_j)}{K(\mathbf{k}_j, \mathbf{k}_{j'})} \div \frac{g(\mathbf{k}_{j'})}{K(\mathbf{k}_j, \mathbf{k}_{j'})} \\
 &= \frac{g(\mathbf{k}_j)}{K(\mathbf{k}_j, \mathbf{k}_{j'})} \times \frac{K(\mathbf{k}_j, \mathbf{k}_{j'})}{g(\mathbf{k}_{j'})} \\
 &= \frac{a_{j'j}}{a_{jj'}} \\
 \implies \mathbf{S} &= \frac{1}{N} \mathbf{A}_{sym} \odot 1/\mathbf{A}_{sym}^\top
 \end{aligned}$$

In Fig. 4, we plot the full training curve of the two versions of Scaled Attention, Scaled Attention \mathbf{S} and Scaled Attention $\alpha \times \text{Asym}$. We observe that the parameterized models with Scaled Attention do converge more quickly and even obtain a slightly higher validation top-1 accuracy of 73.02% for the scalar variant as compared to the standard asymmetric ViT at 72.18%. The final validation loss is also lower at 1.18 and 1.23 respectively.

E.2 Pairwise Absolute Differences of γ_i and γ_j

In Figure 5, we provide the plot of the absolute differences of the coordinates of $\frac{\widetilde{\mathbf{K}}_\varphi \hat{\mathbf{a}}_d}{N \hat{\mathbf{a}}_d}$ in all 12 layers of a ViT-tiny model as elaborated in Section 2.2.2. This would be a constant vector within our framework and the plots provide empirical evidence to justify our claim. In all of the layers, the means are noticeably close to 0 and the standard deviations are also small suggesting that we indeed recovered a constant vector.

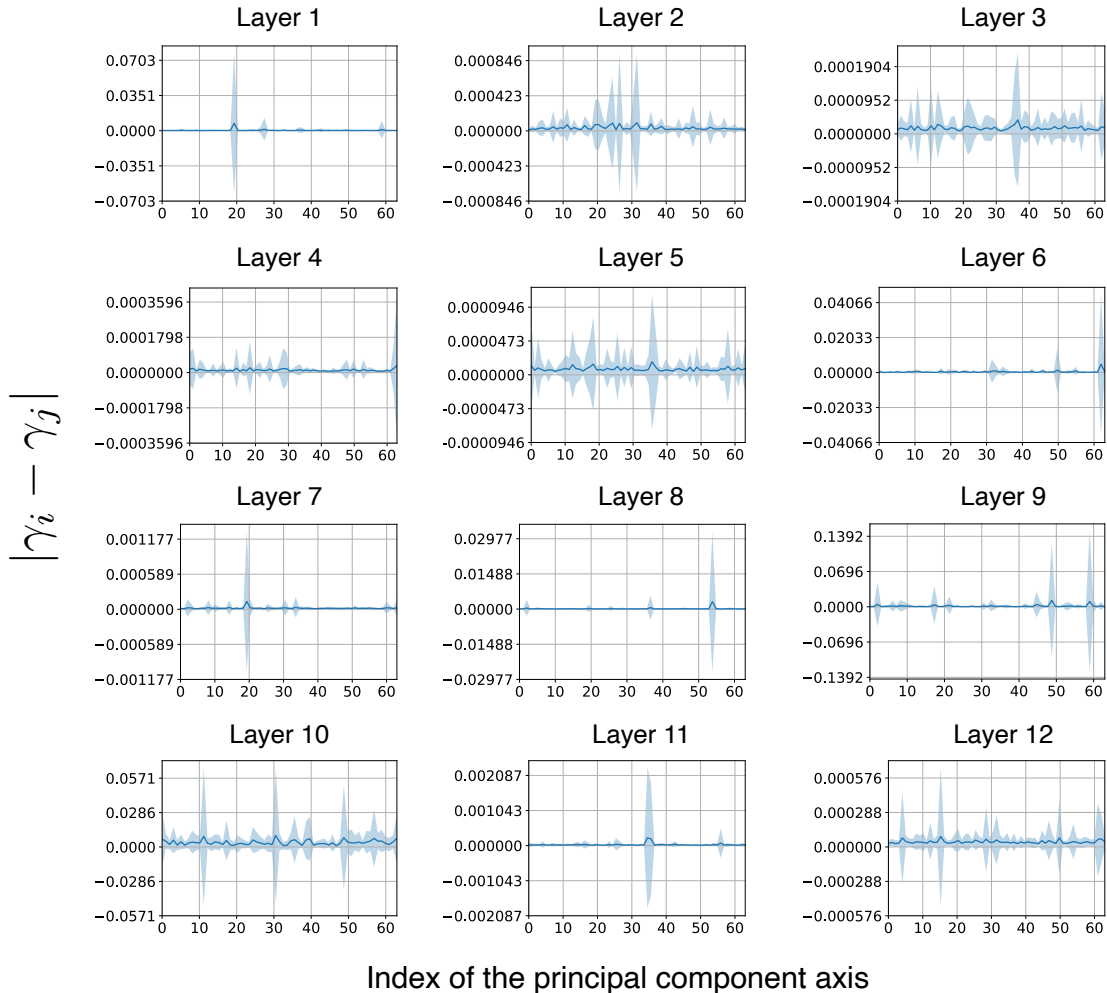


Figure 5: Plot of the mean and standard deviation of the differences in coordinate values of constant vector $\mathbf{1}\lambda_d$ for $d = 1, \dots, D_v$ for all 12 layers of a ViT-tiny model. The mean should be 0 with small standard deviations when $v_{dj} \approx \frac{a_{dj}}{g(\mathbf{k}_j)} - \frac{1}{N} \sum_{j'=1}^N \frac{a_{dj'}}{g(\mathbf{k}_{j'})}$.

E.3 ImageNet-C Results by Corruption Type

In Table 4, we provide the full results of various RPC-SymViT models against the standard SymViT on ImageNet-C for all corruption types averaged over the 5 severity levels. In all types, except for Zoom Blur, the RPC-SymViT model with 6 iterations in the 1st layer outperforms SymViT.

E.4 Square Attack

Square attack [2] is a score-based black box attack that does not use local gradient information, hence it is not affected by gradient masking. It operates based on a random search scheme that modifies square-shaped regions such that at each iteration, the perturbation lies approximately at the boundary of the feasible set. We evaluate our RPC-SymViT(6iter/layer1) variant on square attacked ImageNet-1K validation set and compare it to the baseline. Our result of

Table 4: Top-1 accuracy (%) and mean corruption error (mCE) of all RPC-SymViT variants and SymViT on each corruption type in ImageNet-C. RPC-SymViT (n iter/layer1) applies n PAP iterations only at the first layer. RPC-SymViT (n iter/all-layer) applies n PAP iterations at all layers.

Corruption Type	Model/ Metric	SymViT	RPC-SymViT (2iter/all-layer)	RPC-SymViT (4iter/layer1)	RPC-SymViT (5iter/layer1)	RPC-SymViT (6iter/layer1)
Brightness	Top-1 \uparrow	63.21	62.97	63.74	64.19	64.31
	mCE \downarrow	65.16	65.69	64.22	63.43	63.22
Contrast	Top-1 \uparrow	50.25	49.59	49.30	49.84	50.18
	mCE \downarrow	58.53	59.08	59.42	58.79	58.39
Defocus Blur	Top-1 \uparrow	35.47	35.61	35.54	35.26	36.38
	mCE \downarrow	78.71	78.53	78.62	78.96	77.59
Elastic Transform	Top-1 \uparrow	44.26	44.52	44.68	44.84	44.72
	mCE \downarrow	86.28	85.87	85.63	85.38	85.56
Fog	Top-1 \uparrow	42.72	45.49	46.03	46.59	46.40
	mCE \downarrow	69.91	66.53	65.87	65.19	65.42
Frost	Top-1 \uparrow	44.55	45.06	45.93	46.24	46.27
	mCE \downarrow	67.08	66.46	65.41	65.04	65.01
Gaussian Noise	Top-1 \uparrow	40.97	41.64	42.22	41.67	42.51
	mCE \downarrow	66.59	65.84	65.19	65.80	64.85
Glass Blur	Top-1 \uparrow	27.79	28.12	28.48	27.87	28.05
	mCE \downarrow	87.39	87.00	86.56	87.30	87.07
Impulse Noise	Top-1 \uparrow	38.56	38.98	40.24	39.46	40.33
	mCE \downarrow	66.59	66.14	64.77	65.61	64.67
JPEG Compression	Top-1 \uparrow	46.28	46.23	47.92	48.41	48.63
	mCE \downarrow	88.58	88.65	85.87	85.06	84.70
Motion Blur	Top-1 \uparrow	40.47	40.00	41.72	41.81	42.22
	mCE \downarrow	75.75	76.43	74.16	74.04	73.51
Pixelate	Top-1 \uparrow	39.36	39.81	41.13	41.86	42.25
	mCE \downarrow	84.47	83.84	82.01	81.00	80.45
Shot Noise	Top-1 \uparrow	38.83	39.20	39.52	39.03	39.71
	mCE \downarrow	68.38	67.98	67.61	68.16	67.40
Snow	Top-1 \uparrow	38.27	37.87	38.75	39.12	38.90
	mCE \downarrow	71.22	71.67	70.66	70.23	70.48
Zoom Blur	Top-1 \uparrow	30.69	29.49	29.97	30.20	30.48
	mCE \downarrow	86.82	88.32	87.72	87.43	87.08

the top-1 and top-5 accuracy in Table 5 illustrates that the effectiveness of RPC-Attention against adversarial attacks is not solely due to a form gradient masking as we still significantly outperform the baseline on square.

Table 5: Top-1 and Top-5 accuracy (%) of RPC-SymViT(6iter/layer1) and baseline SymViT on square attacked ImageNet-1K validation data. RPC-SymViT (n iter/layer1) applies n PAP iterations only at the first layer.

Model	Square attack	
	Top-1 \uparrow	Top-5 \uparrow
SymViT (baseline)	41.50	79.79
RPC-SymViT (6iter/layer1)	43.64	80.81

Table 6: Mean accuracy (%) and mean Intersection-Over-Union (IOU) of RPC-SymViT and SymViT on clean ADE20K and corrupted ADE20K dataset. RPC-SymViT (n iter/layer1) applies n PAP iterations only at the first layer. RPC-SymViT (n iter/all-layer) applies n PAP iterations at all layers.

Model	ADE20K		Corrupted ADE20K	
	Mean Acc. \uparrow	Mean IOU \uparrow	Mean Acc. \uparrow	Mean IOU \uparrow
SymViT	44.27	34.00	14.85	10.47
RPC-SymViT (4iter/layer1)	45.61	34.69	16.06	11.47
RPC-SymViT (5iter/layer1)	45.51	34.63	16.15	11.35
RPC-SymViT (6iter/layer1)	45.27	34.24	16.44	11.60
RPC-SymViT (2iter/all-layer)	43.61	33.5	15.04	10.64

E.5 Results on ADE20K Image Segmentation

We further evaluate the benefits of our method by implementing RPC-Attention in a Segmenter model [57] and providing results on the ADE20K image segmentation task [79] in Table 6. We report the Mean Accuracy and Mean Intersection-Over-Union (IOU) for a Segmenter with a RPC-SymViT backbone and compare it against a baseline SymViT backbone. To assess the robustness of each model, we corrupt the ADE20K dataset with the same 15 corruption types in ImageNet-C and report the same metrics averaged over all corruption types in Table 6 as well. Details of our implementation can be found in Appendix A.3. On both datasets, RPC-SymViT outperforms the baseline substantially.

E.6 Results on RPC-SymViT-small

To show that RPC-Attention is not limited to small-scale models, we experiment on a larger model, SymViT-small with 12 transformer layers, 6 heads per layer and a hidden dimension of 384. We train a SymViT-small baseline on ImageNet-1K for 300 epochs and finetune that model for 100 epochs with RPC-Attention in the first layer using 4 iterations with the hyperparameters $\lambda = 4$ and $\mu = ND/4\|\mathbf{K}\|_1$. We refer to this model as RPC-SymViT-small (4iter/layer1). We compare our RPC-SymViT-small with the baseline on the same standard robustness benchmarks as before, ImageNet-C, ImageNet-A, ImageNet-O and ImageNet-R as well as on white box attacks PGD and FGSM with the highest perturbation budgets. These

Table 7: Top-1, Top-5 accuracy (%) , mean corruption error (mCE), and area under the precision-recall curve (AUPR) of RPC-SymViT-small and SymViT-small on clean ImageNet-1K data and popular standard robustness benchmarks for image classification. RPC-SymViT-small (n iter/layer1) applies n PAP iterations only at the first layer.

Model	IN-1K		IN-R	IN-A	IN-C		IN-O
	Top-1 \uparrow	Top-5 \uparrow	Top-1 \uparrow	Top-1 \uparrow	Top-1 \uparrow	mCE \downarrow	AUPR \uparrow
SymViT-small (baseline)	78.72	94.39	38.33	17.43	54.32	58.24	20.06
RPC-SymViT-small (4iter/layer1)	78.84	94.49	38.08	17.52	54.48	58.00	20.30

Table 8: Top-1 and Top-5 accuracy (%) of RPC-SymViT-small and SymViT-small on PGD and FGSM attacked ImageNet-1K validation data with the highest perturbation budget. RPC-SymViT (n iter/layer1) applies n PAP iterations only at the first layer.

Model	PGD		FGSM	
	Top-1 \uparrow	Top-5 \uparrow	Top-1 \uparrow	Top-5 \uparrow
SymViT-small (baseline)	41.47	71.53	8.35	19.99
RPC-SymViT-small (4iter/layer1)	41.94	71.59	8.94	20.70

results are in Table 7 and 8 respectively and show that RPC-Attention is also effective in SymViT-small.

E.7 Results on RPC-Attention in FAN

To validate that our RPC-Attention is also complementary with SOTA transformer models and can be combined with those methods to improve the SOTA results, we have conducted additional experiments in which we incorporate our RPC-Attention with FAN [80]. FAN is one of the top transformer models that obtain SOTA results on accuracy and robustness. A FAN model augments the MLP layer that follows the standard self-attention with a new channel attention (CA) block. This CA computes an attention matrix along the channel dimension, taking advantage of the feature covariance and allowing the model to filter out irrelevant information.

We use the FAN-ViT-tiny (FAN-tiny) variant with a symmetric attention for training. In our RPC-Attention + FAN (RPC-FAN-tiny), we replace the attention blocks in the first layer of FAN with our RPC-Attention that runs 4 PAP iterations with hyperparameter values of $\lambda = 4$ and $\mu = ND/4\|\mathbf{K}\|_1$. Both our RPC-FAN-tiny and the baseline FAN-tiny are trained for 300 epochs on the ImageNet-1K object classification task. We summarize our results in Tables 9 and 10. RPC-FAN-tiny outperforms the baseline FAN-tiny on all evaluated benchmarks, including ImageNet-1k, ImageNet-R, and ImageNet-A. Additionally, on PGD and FGSM attacked data, RPC-FAN-tiny significantly outperforms FAN-tiny by over 3%.

Table 9: Top-1, top-5 accuracy (%) of RPC-FAN-tiny and FAN-tiny on clean ImageNet-1K data and popular standard robustness benchmarks for image classification. RPC-FAN-tiny (n iter/layer1) applies n PAP iterations only at the first layer.

Model	IN-1K		IN-R	IN-A
	Top-1 \uparrow	Top-5 \uparrow	Top-1 \uparrow	Top-1 \uparrow
FAN-tiny (baseline)	77.89	94.20	41.79	13.40
RPC-FAN-tiny (4iter/layer1)	77.98	94.27	42.02	13.55

Table 10: Top-1 and top-5 accuracy (%) of RPC-FAN-tiny and FAN-tiny on PGD and FGSM attacked ImageNet-1K validation data with the highest perturbation budget. RPC-FAN-ViT (n iter/layer1) applies n PAP iterations only at the first layer.

Model	PGD		FGSM	
	Top-1 \uparrow	Top-5 \uparrow	Top-1 \uparrow	Top-5 \uparrow
FAN-tiny (baseline)	2.92	4.86	32.01	61.72
RPC-FAN-tiny (4iter/layer1)	6.25	10.01	35.12	63.40

Table 11: Flop per sample, run time per sample, memory and number of parameters of each RPC-SymViT variant compared to the SymViT baseline. RPC-SymViT (n iter/layer1) applies n PAP iterations only at the first layer. RPC-SymViT (n iter/all-layer) applies n PAP iterations at all layers.

Model	Flop/Sample	Sec/Sample (Training)	Sec/Sample (Test)	Memory (Training)	Memory (Test)	Parameters
SymViT (baseline)	1.17M	0.079	0.010	1435MB	1181MB	5.2M
RPC-SymViT (4iter/layer1)	1.22M	0.082	0.010	1441MB	1181MB	5.2M
RPC-SymViT (5iter/layer1)	1.23M	0.084	0.010	1443MB	1181MB	5.2M
RPC-SymViT (6iter/layer1)	1.25M	0.085	0.011	1443MB	1181MB	5.2M
RPC-SymViT (2iter/layer)	1.35M	0.092	0.017	1461MB	1181MB	5.2M

E.8 Computational Efficiency

A possible limitation of introducing an iterative scheme into a deep model is a significant increase in computational overhead. We aim to alleviate that concern by providing the number of flops per sample, run time per sample, memory and number of parameters of each RPC-SymViT variant and the SymViT baseline during both training and test time in Table 11. We observe that RPC-Attention is comparable to the baseline softmax attention across all metrics at test time while only slightly less efficient than the baseline in terms of the number of flops, run time per sample, and memory during training.

Table 12: Top-1, top-5 accuracy (%) and AUPR of an implementation of RPC-Attention on asymmetric attention evaluated on ImageNet-1K validation set, ImageNet-R, ImageNet-A and ImageNet-O. These results are compared to the standard asymmetric ViT.

Model	IN-1K		IN-R	IN-A	IN-O
	Top-1 \uparrow	Top-5 \uparrow	Top-1 \uparrow	Top-1 \uparrow	AUPR \uparrow
ViT	72.11	90.97	32.41	7.65	17.36
RPC-AsymViT (4iter/layer1)	72.34	91.12	32.23	7.75	17.54
RPC-AsymViT (Sym/Asym)	72.34	91.38	32.79	7.23	17.58

E.9 Results on Robust Asymmetric Attention

In this section, we report the results of extending the RPC-SymViT model to the asymmetric attention. However, as the PAP Algorithm. 1 is not designed for multiple data matrices, it is not as effective in the asymmetric case. We implement two variations of the algorithm in an asymmetric attention ViT-tiny with 12 layers. In the 4iter/layer1 version, similar to the symmetric attention case, we run 4 iterations of the algorithm only in the first layer of the model by replacing $\text{Softmax}(\mathbf{K} - \mathbf{S}_{k+1} - \mu^{-1}\mathbf{Y}_k, \mathbf{K} - \mathbf{S}_{k+1} - \mu^{-1}\mathbf{Y}_k)$ with $\text{Softmax}(\mathbf{Q}, \mathbf{K} - \mathbf{S}_{k+1} - \mu^{-1}\mathbf{Y}_k)$. For the second version, labeled Sym/Asym, we run the algorithm for 4 iterations in a symmetric attention mechanism in the first layer, followed by the standard asymmetric attention in layers 2 to 12. We compare these RPC-AsymViT models to the asymmetric softmax attention ViT.

As we can see from Table 12, both variants only improve slightly over the benchmark on most of the corrupted datasets. Such a result confirms our intuition that the ADMM algorithm does not extend easily to multiple corrupted matrices as it only solves an objective function involving a single low-rank data matrix and its sparse corruption matrix.

F Further Discussion on Related Works

[11] provides a new perspective by emphasizing the asymmetry of the softmax kernel and recovers the self-attention mechanism from an asymmetric Kernel Singular Value Decomposition (KSVD) using the duality of the optimization problem. Separately, our kernel PCA perspective derives softmax attention and addresses the asymmetry of attention through a projection of the query vectors in feature space. While there are similarities between KSVD and kernel PCA, in the sense of finding low rank approximations and low dimensional representations of the data, the primal objective functions are different and we do not need to consider the dual form. Another related work views transformers from the perspective of Support Vector Machines [61]. Though, kernel PCA can be formulated in a similar fashion as a least squares SVM problem as explained in [59], our work focuses on the forward pass of attention and show that it can recover a kernel PCA solution. In contrast, [59] examines the backward pass and optimization geometry of an attention layer towards a hard margin SVM solution that separates optimal tokens from non-optimal ones, under certain assumptions of the loss function, initial conditions, and certain SVM constraints. Furthermore, using our framework, we are able to predict the exact explicit form of the value matrix in self-attention, demonstrating that

this matrix captures the eigenvectors of the Gram matrix of the key vectors in a feature space. To the best of our knowledge, our work is the first to show this insight.

G Broader Impacts

Our research improves both clean data processing and robust performance, especially in areas with significant social relevance. Specifically, we demonstrate enhanced results in image segmentation, benefiting self-driving cars, and language modeling, enhancing AI chatbot assistants. We show notable improvements in resisting adversarial attacks, aiming to protect crucial AI systems from malicious actors. Additionally, we achieve competitive performance in language modeling with contaminated data, which is often encountered in real-world situations. Despite the potential for AI misuse, our research presents substantial advancements in fundamental architectures and theory, which we hope will inspire further socially beneficial developments.

References

- [1] R. Al-Rfou, D. Choe, N. Constant, M. Guo, and L. Jones. Character-level language modeling with deeper self-attention. In *Proceedings of the AAAI Conference on Artificial Intelligence*, volume 33, pages 3159–3166, 2019.
- [2] M. Andriushchenko, F. Croce, N. Flammarion, and M. Hein. Square attack: a query-efficient black-box adversarial attack via random search, 2020.
- [3] A. Baevski and M. Auli. Adaptive input representations for neural language modeling. In *International Conference on Learning Representations*, 2019.
- [4] D. Bahdanau, K. Cho, and Y. Bengio. Neural machine translation by jointly learning to align and translate. *arXiv preprint arXiv:1409.0473*, 2014.
- [5] S. Bhojanapalli, A. Chakrabarti, D. Glasner, D. Li, T. Unterthiner, and A. Veit. Understanding robustness of transformers for image classification. *CoRR*, abs/2103.14586, 2021.
- [6] C. Bishop. Pattern recognition and machine learning. *Springer google schola*, 2:531–537, 2006.
- [7] T. Brown, B. Mann, N. Ryder, M. Subbiah, J. D. Kaplan, P. Dhariwal, A. Neelakantan, P. Shyam, G. Sastry, A. Askell, S. Agarwal, A. Herbert-Voss, G. Krueger, T. Henighan, R. Child, A. Ramesh, D. Ziegler, J. Wu, C. Winter, C. Hesse, M. Chen, E. Sigler, M. Litwin, S. Gray, B. Chess, J. Clark, C. Berner, S. McCandlish, A. Radford, I. Sutskever, and D. Amodei. Language models are few-shot learners. In H. Larochelle, M. Ranzato, R. Hadsell, M. Balcan, and H. Lin, editors, *Advances in Neural Information Processing Systems*, volume 33, pages 1877–1901. Curran Associates, Inc., 2020.
- [8] E. J. Candès, X. Li, Y. Ma, and J. Wright. Robust principal component analysis? *Journal of the ACM (JACM)*, 58(3):1–37, 2011.

- [9] N. Carlini and D. A. Wagner. Towards evaluating the robustness of neural networks. *CoRR*, abs/1608.04644, 2016.
- [10] L. Chen, K. Lu, A. Rajeswaran, K. Lee, A. Grover, M. Laskin, P. Abbeel, A. Srinivas, and I. Mordatch. Decision transformer: Reinforcement learning via sequence modeling. *Advances in neural information processing systems*, 34:15084–15097, 2021.
- [11] Y. Chen, Q. Tao, F. Tonin, and J. A. K. Suykens. Primal-attention: Self-attention through asymmetric kernel svd in primal representation, 2023.
- [12] K. M. Choromanski, V. Likhoshesterov, D. Dohan, X. Song, A. Gane, T. Sarlos, P. Hawkins, J. Q. Davis, A. Mohiuddin, L. Kaiser, D. B. Belanger, L. J. Colwell, and A. Weller. Rethinking attention with performers. In *International Conference on Learning Representations*, 2021.
- [13] A. Chowdhery, S. Narang, J. Devlin, M. Bosma, G. Mishra, A. Roberts, P. Barham, H. W. Chung, C. Sutton, S. Gehrmann, P. Schuh, K. Shi, S. Tsvyashchenko, J. Maynez, A. Rao, P. Barnes, Y. Tay, N. Shazeer, V. Prabhakaran, E. Reif, N. Du, B. Hutchinson, R. Pope, J. Bradbury, J. Austin, M. Isard, G. Gur-Ari, P. Yin, T. Duke, A. Levskaya, S. Ghemawat, S. Dev, H. Michalewski, X. Garcia, V. Misra, K. Robinson, L. Fedus, D. Zhou, D. Ippolito, D. Luan, H. Lim, B. Zoph, A. Spiridonov, R. Sepassi, D. Dohan, S. Agrawal, M. Omernick, A. M. Dai, T. S. Pillai, M. Pellat, A. Lewkowycz, E. Moreira, R. Child, O. Polozov, K. Lee, Z. Zhou, X. Wang, B. Saeta, M. Diaz, O. Firat, M. Catasta, J. Wei, K. Meier-Hellstern, D. Eck, J. Dean, S. Petrov, and N. Fiedel. Palm: Scaling language modeling with pathways. *Journal of Machine Learning Research*, 24(240):1–113, 2023.
- [14] F. Croce and M. Hein. Reliable evaluation of adversarial robustness with an ensemble of diverse parameter-free attacks, 2020.
- [15] F. De la Torre and M. J. Black. Robust principal component analysis for computer vision. In *Proceedings Eighth IEEE International Conference on Computer Vision. ICCV 2001*, volume 1, pages 362–369. IEEE, 2001.
- [16] J. Devlin, M.-W. Chang, K. Lee, and K. Toutanova. BERT: Pre-training of deep bidirectional transformers for language understanding. In J. Burstein, C. Doran, and T. Solorio, editors, *Proceedings of the 2019 Conference of the North American Chapter of the Association for Computational Linguistics: Human Language Technologies, Volume 1 (Long and Short Papers)*, pages 4171–4186, Minneapolis, Minnesota, June 2019. Association for Computational Linguistics.
- [17] Y. Dong, J.-B. Cordonnier, and A. Loukas. Attention is not all you need: Pure attention loses rank doubly exponentially with depth. In *International Conference on Machine Learning*, pages 2793–2803. PMLR, 2021.
- [18] A. Dosovitskiy, L. Beyer, A. Kolesnikov, D. Weissenborn, X. Zhai, T. Unterthiner, M. Dehghani, M. Minderer, G. Heigold, S. Gelly, J. Uszkoreit, and N. Houlsby. An image is worth 16x16 words: Transformers for image recognition at scale. In *International Conference on Learning Representations*, 2021.

- [19] P. Gabbur, M. Bilkhu, and J. Movellan. Probabilistic attention for interactive segmentation. In M. Ranzato, A. Beygelzimer, Y. Dauphin, P. Liang, and J. W. Vaughan, editors, *Advances in Neural Information Processing Systems*, volume 34, pages 4448–4460. Curran Associates, Inc., 2021.
- [20] R. Gal, Y. Alaluf, Y. Atzmon, O. Patashnik, A. H. Bermano, G. Chechik, and D. Cohen-or. An image is worth one word: Personalizing text-to-image generation using textual inversion. In *The Eleventh International Conference on Learning Representations*, 2023.
- [21] B. Geshkovski, C. Letrouit, Y. Polyanskiy, and P. Rigollet. A mathematical perspective on transformers, 2023.
- [22] B. Geshkovski, C. Letrouit, Y. Polyanskiy, and P. Rigollet. The emergence of clusters in self-attention dynamics, 2024.
- [23] I. Goodfellow, J. Shlens, and C. Szegedy. Explaining and harnessing adversarial examples. In *International Conference on Learning Representations*, 2015.
- [24] D. Hendrycks, S. Basart, N. Mu, S. Kadavath, F. Wang, E. Dorundo, R. Desai, T. Zhu, S. Parajuli, M. Guo, D. Song, J. Steinhardt, and J. Gilmer. The many faces of robustness: A critical analysis of out-of-distribution generalization. *CoRR*, abs/2006.16241, 2020.
- [25] D. Hendrycks and T. G. Dietterich. Benchmarking neural network robustness to common corruptions and perturbations. *CoRR*, abs/1903.12261, 2019.
- [26] D. Hendrycks, K. Zhao, S. Basart, J. Steinhardt, and D. Song. Natural adversarial examples. In *Proceedings of the IEEE/CVF conference on computer vision and pattern recognition*, pages 15262–15271, 2021.
- [27] J. Hewitt and P. Liang. Designing and interpreting probes with control tasks. In *Proceedings of the 2019 Conference on Empirical Methods in Natural Language Processing and the 9th International Joint Conference on Natural Language Processing (EMNLP-IJCNLP)*, pages 2733–2743, Hong Kong, China, Nov. 2019. Association for Computational Linguistics.
- [28] M. Hubert, P. J. Rousseeuw, and K. Vanden Branden. Robpca: a new approach to robust principal component analysis. *Technometrics*, 47(1):64–79, 2005.
- [29] M. Janner, Q. Li, and S. Levine. Offline reinforcement learning as one big sequence modeling problem. *Advances in neural information processing systems*, 34:1273–1286, 2021.
- [30] J. Jumper, R. Evans, A. Pritzel, T. Green, M. Figurnov, O. Ronneberger, K. Tunyasuvunakool, R. Bates, A. Žídek, A. Potapenko, et al. Highly accurate protein structure prediction with alphafold. *Nature*, 596(7873):583–589, 2021.
- [31] A. Katharopoulos, A. Vyas, N. Pappas, and F. Fleuret. Transformers are rnns: Fast autoregressive transformers with linear attention. *CoRR*, abs/2006.16236, 2020.
- [32] S. Khan, M. Naseer, M. Hayat, S. W. Zamir, F. S. Khan, and M. Shah. Transformers in vision: A survey. *ACM computing surveys (CSUR)*, 54(10s):1–41, 2022.

- [33] T. Kojima, S. S. Gu, M. Reid, Y. Matsuo, and Y. Iwasawa. Large language models are zero-shot reasoners. In S. Koyejo, S. Mohamed, A. Agarwal, D. Belgrave, K. Cho, and A. Oh, editors, *Advances in Neural Information Processing Systems*, volume 35, pages 22199–22213. Curran Associates, Inc., 2022.
- [34] K.-H. Lee, O. Nachum, M. S. Yang, L. Lee, D. Freeman, S. Guadarrama, I. Fischer, W. Xu, E. Jang, H. Michalewski, et al. Multi-game decision transformers. *Advances in Neural Information Processing Systems*, 35:27921–27936, 2022.
- [35] Z. Lin, M. Chen, and Y. Ma. The augmented lagrange multiplier method for exact recovery of corrupted low-rank matrices. *arXiv preprint arXiv:1009.5055*, 2010.
- [36] Z. Lin, M. Feng, C. N. dos Santos, M. Yu, B. Xiang, B. Zhou, and Y. Bengio. A STRUCTURED SELF-ATTENTIVE SENTENCE EMBEDDING. In *International Conference on Learning Representations*, 2017.
- [37] Z. Liu, Y. Lin, Y. Cao, H. Hu, Y. Wei, Z. Zhang, S. Lin, and B. Guo. Swin transformer: Hierarchical vision transformer using shifted windows. In *Proceedings of the IEEE/CVF International Conference on Computer Vision*, pages 10012–10022, 2021.
- [38] Y. Lu, Z. Li, D. He, Z. Sun, B. Dong, T. Qin, L. Wang, and T.-Y. Liu. Understanding and improving transformer from a multi-particle dynamic system point of view, 2019.
- [39] A. Madry, A. Makelov, L. Schmidt, D. Tsipras, and A. Vladu. Towards deep learning models resistant to adversarial attacks. In *International Conference on Learning Representations*, 2018.
- [40] X. Mao, G. Qi, Y. Chen, X. Li, R. Duan, S. Ye, Y. He, and H. Xue. Towards robust vision transformer, 2022.
- [41] S. Merity, C. Xiong, J. Bradbury, and R. Socher. Pointer sentinel mixture models. *CoRR*, abs/1609.07843, 2016.
- [42] J. Morris, E. Lifland, J. Y. Yoo, J. Grigsby, D. Jin, and Y. Qi. Textattack: A framework for adversarial attacks, data augmentation, and adversarial training in nlp. In *Proceedings of the 2020 Conference on Empirical Methods in Natural Language Processing: System Demonstrations*, pages 119–126, 2020.
- [43] M. Nguyen and F. Torre. Robust kernel principal component analysis. *Advances in Neural Information Processing Systems*, 21, 2008.
- [44] N. Papernot, F. Faghri, N. Carlini, I. Goodfellow, R. Feinman, A. Kurakin, C. Xie, Y. Sharma, T. Brown, A. Roy, A. Matyasko, V. Behzadan, K. Hambardzumyan, Z. Zhang, Y.-L. Juang, Z. Li, R. Sheatsley, A. Garg, J. Uesato, W. Gierke, Y. Dong, D. Berthelot, P. Hendricks, J. Rauber, and R. Long. Technical report on the cleverhans v2.1.0 adversarial examples library. *arXiv preprint arXiv:1610.00768*, 2018.
- [45] A. Parikh, O. Täckström, D. Das, and J. Uszkoreit. A decomposable attention model for natural language inference. In J. Su, K. Duh, and X. Carreras, editors, *Proceedings of the*

- 2016 *Conference on Empirical Methods in Natural Language Processing*, pages 2249–2255, Austin, Texas, Nov. 2016. Association for Computational Linguistics.
- [46] S. Paul and P. Chen. Vision transformers are robust learners. *CoRR*, abs/2105.07581, 2021.
- [47] K. Pearson. Liii. on lines and planes of closest fit to systems of points in space. *The London, Edinburgh, and Dublin philosophical magazine and journal of science*, 2(11):559–572, 1901.
- [48] A. Radford, J. W. Kim, C. Hallacy, A. Ramesh, G. Goh, S. Agarwal, G. Sastry, A. Askell, P. Mishkin, J. Clark, et al. Learning transferable visual models from natural language supervision. In *International Conference on Machine Learning*, pages 8748–8763. PMLR, 2021.
- [49] A. Radford, K. Narasimhan, T. Salimans, and I. Sutskever. Improving language understanding by generative pre-training. *OpenAI report*, 2018.
- [50] A. Radford, J. Wu, R. Child, D. Luan, D. Amodei, and I. Sutskever. Language models are unsupervised multitask learners. *OpenAI blog*, 1(8):9, 2019.
- [51] C. Raffel, N. Shazeer, A. Roberts, K. Lee, S. Narang, M. Matena, Y. Zhou, W. Li, and P. J. Liu. Exploring the limits of transfer learning with a unified text-to-text transformer. *Journal of Machine Learning Research*, 21(140):1–67, 2020.
- [52] R. M. Rao, J. Liu, R. Verkuil, J. Meier, J. Canny, P. Abbeel, T. Sercu, and A. Rives. Msa transformer. In M. Meila and T. Zhang, editors, *Proceedings of the 38th International Conference on Machine Learning*, volume 139 of *Proceedings of Machine Learning Research*, pages 8844–8856. PMLR, 18–24 Jul 2021.
- [53] A. Rives, J. Meier, T. Sercu, S. Goyal, Z. Lin, J. Liu, D. Guo, M. Ott, C. L. Zitnick, J. Ma, et al. Biological structure and function emerge from scaling unsupervised learning to 250 million protein sequences. *Proceedings of the National Academy of Sciences*, 118(15), 2021.
- [54] M. E. Sander, P. Ablin, M. Blondel, and G. Peyré. Sinkformers: Transformers with doubly stochastic attention. *CoRR*, abs/2110.11773, 2021.
- [55] I. Schlag, K. Irie, and J. Schmidhuber. Linear transformers are secretly fast weight programmers. In *Proc. Int. Conf. on Machine Learning (ICML)*, Virtual only, July 2021.
- [56] H. Shi, J. GAO, H. Xu, X. Liang, Z. Li, L. Kong, S. M. S. Lee, and J. Kwok. Revisiting over-smoothing in BERT from the perspective of graph. In *International Conference on Learning Representations*, 2022.
- [57] R. Strudel, R. Garcia, I. Laptev, and C. Schmid. Segmenter: Transformer for semantic segmentation, 2021.
- [58] A. Subramanya, A. Saha, S. A. Koohpayegani, A. Tejankar, and H. Pirsiavash. Backdoor attacks on vision transformers, 2022.

- [59] J. Suykens, T. Van Gestel, J. Vandewalle, and B. De Moor. A support vector machine formulation to pca analysis and its kernel version. *IEEE Transactions on Neural Networks*, 14(2):447–450, 2003.
- [60] B. Tang and D. S. Matteson. Probabilistic transformer for time series analysis. In A. Beygelzimer, Y. Dauphin, P. Liang, and J. W. Vaughan, editors, *Advances in Neural Information Processing Systems*, 2021.
- [61] D. A. Tarzanagh, Y. Li, C. Thrampoulidis, and S. Oymak. Transformers as support vector machines. *arXiv preprint arXiv:2308.16898*, 2023.
- [62] I. Tenney, D. Das, and E. Pavlick. BERT rediscovers the classical NLP pipeline. In *Proceedings of the 57th Annual Meeting of the Association for Computational Linguistics*, pages 4593–4601, Florence, Italy, July 2019. Association for Computational Linguistics.
- [63] H. Touvron, M. Cord, M. Douze, F. Massa, A. Sablayrolles, and H. Jégou. Training data-efficient image transformers & distillation through attention. *CoRR*, abs/2012.12877, 2020.
- [64] H. Touvron, M. Cord, M. Douze, F. Massa, A. Sablayrolles, and H. Jegou. Training data-efficient image transformers & distillation through attention. In M. Meila and T. Zhang, editors, *Proceedings of the 38th International Conference on Machine Learning*, volume 139 of *Proceedings of Machine Learning Research*, pages 10347–10357. PMLR, 18–24 Jul 2021.
- [65] F. Tramèr and D. Boneh. Adversarial training and robustness for multiple perturbations. *CoRR*, abs/1904.13000, 2019.
- [66] Y.-H. H. Tsai, S. Bai, M. Yamada, L.-P. Morency, and R. Salakhutdinov. Transformer dissection: An unified understanding for transformer’s attention via the lens of kernel. In K. Inui, J. Jiang, V. Ng, and X. Wan, editors, *Proceedings of the 2019 Conference on Empirical Methods in Natural Language Processing and the 9th International Joint Conference on Natural Language Processing (EMNLP-IJCNLP)*, pages 4344–4353, Hong Kong, China, Nov. 2019. Association for Computational Linguistics.
- [67] J. Uesato, B. O’donoghue, P. Kohli, and A. Oord. Adversarial risk and the dangers of evaluating against weak attacks. In *International Conference on Machine Learning*, pages 5025–5034. PMLR, 2018.
- [68] A. Vaswani, N. Shazeer, N. Parmar, J. Uszkoreit, L. Jones, A. N. Gomez, Ł. Kaiser, and I. Polosukhin. Attention is all you need. In *Advances in neural information processing systems*, pages 5998–6008, 2017.
- [69] J. Vig and Y. Belinkov. Analyzing the structure of attention in a transformer language model. In *Proceedings of the 2019 ACL Workshop BlackboxNLP: Analyzing and Interpreting Neural Networks for NLP*, pages 63–76, Florence, Italy, Aug. 2019. Association for Computational Linguistics.

- [70] E. Voita, D. Talbot, F. Moiseev, R. Sennrich, and I. Titov. Analyzing multi-head self-attention: Specialized heads do the heavy lifting, the rest can be pruned. In *Proceedings of the 57th Annual Meeting of the Association for Computational Linguistics*, pages 5797–5808, Florence, Italy, July 2019. Association for Computational Linguistics.
- [71] P. Wang, W. Zheng, T. Chen, and Z. Wang. Anti-oversmoothing in deep vision transformers via the fourier domain analysis: From theory to practice. In *International Conference on Learning Representations*, 2022.
- [72] S. Wang, B. Z. Li, M. Khabsa, H. Fang, and H. Ma. Linformer: Self-attention with linear complexity. *CoRR*, abs/2006.04768, 2020.
- [73] Z. Wang and J. Sun. TransTab: Learning Transferable Tabular Transformers Across Tables. In *Advances in Neural Information Processing Systems (NeurIPS 2022)*, 2022.
- [74] Z. Yang, Z. Dai, Y. Yang, J. Carbonell, R. R. Salakhutdinov, and Q. V. Le. Xlnet: Generalized autoregressive pretraining for language understanding. In H. Wallach, H. Larochelle, A. Beygelzimer, F. d'Alché-Buc, E. Fox, and R. Garnett, editors, *Advances in Neural Information Processing Systems*, volume 32. Curran Associates, Inc., 2019.
- [75] X. Yuan and J. Yang. Sparse and low-rank matrix decomposition via alternating direction methods. *preprint*, 12(2), 2009.
- [76] S. Zhang and Y. Feng. Modeling concentrated cross-attention for neural machine translation with Gaussian mixture model. In M.-F. Moens, X. Huang, L. Specia, and S. W.-t. Yih, editors, *Findings of the Association for Computational Linguistics: EMNLP 2021*, pages 1401–1411, Punta Cana, Dominican Republic, Nov. 2021. Association for Computational Linguistics.
- [77] S. Zhang, L. Yao, A. Sun, and Y. Tay. Deep learning based recommender system: A survey and new perspectives. *ACM Computing Surveys (CSUR)*, 52(1):1–38, 2019.
- [78] Q. Zheng, A. Zhang, and A. Grover. Online decision transformer. In *international conference on machine learning*, pages 27042–27059. PMLR, 2022.
- [79] B. Zhou, H. Zhao, X. Puig, S. Fidler, A. Barriuso, and A. Torralba. Scene parsing through ade20k dataset. In *2017 IEEE Conference on Computer Vision and Pattern Recognition (CVPR)*, pages 5122–5130, 2017.
- [80] D. Zhou, Z. Yu, E. Xie, C. Xiao, A. Anandkumar, J. Feng, and J. M. Alvarez. Understanding the robustness in vision transformers, 2022.
- [81] L. Zhuang, L. Wayne, S. Ya, and Z. Jun. A robustly optimized BERT pre-training approach with post-training. In S. Li, M. Sun, Y. Liu, H. Wu, K. Liu, W. Che, S. He, and G. Rao, editors, *Proceedings of the 20th Chinese National Conference on Computational Linguistics*, pages 1218–1227, Huhhot, China, Aug. 2021. Chinese Information Processing Society of China.